Coexisting solutions and bifurcations in mechanical oscillators with backlash

Christopher K. Halse [a,1], R. Eddie Wilson [b], Mario di Bernardo [b,c] and Martin E. Homer [b]

[a] *Romax Technology, Rutherford House, Nottingham Science and Technology Park, NG7 2PZ, U.K.*

[b] *Bristol Centre for Applied Nonlinear Mathematics, University of Bristol, Bristol BS8 1TR, U.K.*

[c] *Department of Systems and Computer Science, University of Naples Federico II, Naples, Italy*

Abstract

Lightly damped geared systems have been shown to exhibit unwanted noise and vibration problems. We present a nonlinear analysis of this behaviour, based on freeplay. We derive a simple model of a pair of meshing spur gears as a single degree of freedom oscillator with backlash. We consider the behaviour of such a system with low damping, and with both large finite and infinite stiffness values. We show that the solution where the gears remain permanently in contact can coexist with many other stable rattling solutions which we compute analytically. We calculate the regions of existence and stability of the families of rattling solutions on two-parameter bifurcation diagrams, and show that to leading order the large finite and infinite stiffness models give the same results. We provide numerical simulation to support our analysis, and we also draw practical conclusions for machine design.

1 Introduction

Play or backlash is an omnipresent reality in engineering. Any mechanical system with joints may suffer from play between the components, which may change with temperature or wear. Backlash oscillations have been shown to give rise to undesirable noise and vibration (N&V) problems in many engineering systems; one particular example is in gearing mechanisms [1–3]. It is

[1] Gratefully acknowledges the support of a CASE award from Jaguar Cars and the Engineering and Physical Sciences Research Council.

impossible to operate gears which mesh perfectly. Rather, it is essential to have a small gap between the trailing face of one tooth and the leading face of the next, known as the backlash (or freeplay), so as to ensure that gears do not jam. Because gears can consequently lose contact, there is a range of relative rotational displacements for which there is no torque transfer between them.

Indeed, in lightly damped, lightly loaded quasi-steady operation, a small amount of oscillatory forcing can excite modes where gears rattle by repeatedly losing and re-establishing contact. The problem of gear rattle excited by parametric forcing, due to stiffness varying at the meshing frequency, is well studied. In contrast, this paper performs a detailed analysis of rattle where right hand side forcing effects are introduced, and the parametric stiffness effect is ignored. One particular application of this model is the Roots blower vacuum pump [4–6], where tiny amounts of eccentricity in the gear mounting introduce a forcing effect which acts at the gross rotation rate of the gears. In the automotive driveline [7,8], a similar effect occurs in the unloaded (i.e. unselected) gear pairs of a manual transmission, and is excited by the torque cycle of the engine.

Backlash oscillations, however, can be found in much more general mechanical systems, for example, rolling mills [9], rotors [10], aeroelastic control systems [11], and even electrical relays [12]. Currently there is no full explanation of the mechanisms leading to the onset of bifurcations and chaos in backlash systems. It has been shown through extensive numerical simulations that backlash systems can exhibit complicated behaviour. The occurrence of chaotic behaviour in a backlash system is discussed in [13] mainly through numerical simulations. The possible bifurcations are examined in more detail in [14] and [15], with numerical techniques. Experiments demonstrating the validity of the results obtained using simple models of backlash oscillators are shown in [16]. The bifurcation scenarios leading to chaotic behaviour are studied numerically in [17].

We will model the backlash with a piecewise linear (PWL) restoring force. We shall present analytical and numerical evidence that this nonlinearity gives rise to coexisting periodic solutions, both ‘silent’ and ‘noisy’ that can explain the typical N&V problems of intermittency (a single machine behaves inconsistently) and sensitive dependence on parameters (apparently identical machines behave differently). It has been pointed out that unwanted dynamics are often associated with coexisting solutions, which are therefore particularly interesting from a design perspective. Specifically, a large enough disturbance may cause the system to be perturbed into the basin of attraction of a solution not accounted for by a linear analysis. This paper shows that there may be large numbers of these coexisting solutions for typical operating parameters.

We construct explicit existence and stability criteria for two classes of rattling periodic orbit, both for a piecewise linear model of backlash with finite stiffness, and for the impacting infinite stiffness limit. We show that, to leading order in the small damping parameter, the existence and stability criteria for the two models are the same. Moreover, we perform an analytical bifurcation analysis in the finite and infinite stiffness cases, considering both standard bifurcations [18] as well as those unique to non-smooth systems [19,20], in order to explore the dynamics as design parameters are varied. Once again, we show that the two backlash models are equivalent. Further, we support our analytical calculations with numerical simulation, and draw practical conclusions for machine design.

The rest of the paper is outlined as follows. In Section 2 we derive the equations of motion for a simple pair of meshing spur gears, with particular reference to the Roots blower vacuum pump problem. This application motivates the small damping, lightly loaded, large stiffness limit which is analysed in the rest of the paper. However, the model we derive applies across a wide range of other lightly loaded geared systems and indeed to more general problems with a backlash nonlinearity. In Sec. 3 we derive bounds on physical parameters for the existence of a silent solution, where the gears remain permanently in contact. In Sec. 4 we motivate parameter scalings and discuss two different ways of dealing with the backlash nonlinearity when the stiffness is large. The first retains a large finite stiffness value whereas the second takes an infinite stiffness limit where contact is modelled by impacts. In Sec. 5 we describe the methods used to construct nonlinear rattling solutions and we determine their stability. We then proceed to use these methods to construct analytical existence and stability criteria for two families of periodic solutions. In Section 6 we consider solutions which contact one side of the backlash once per period, while in Sec. 7 we consider solutions which contact each side of the backlash once per period. In each case we compare both the finite stiffness and the impacting contact model, and we present two-parameter bifurcation diagrams that summarise our findings. We also interpret the significance of the results from the point of view of machine design. Finally, in Sec. 8, we present conclusions and identify areas for further work.

2 Modelling

We shall derive a model with specific reference to N&V problems in the gearing mechanism of Roots blower vacuum pumps. However, we believe that the equations derived here are applicable to much wider classes of backlash oscillators.

A Roots blower pump [4–6] is made up of two involute steel rotors (denoted by

X and Y), rigidly attached to two counter-rotating parallel shafts. One shaft (the X-shaft) is driven by means of a motor, while the other (the Y-shaft) is driven only by means of a gearing mechanism between the two shafts. A schematic diagram is shown in Fig. 1. Note that contact is through the gears only, not through the lobes of the rotors. When the gear teeth are in contact, we suppose that each assembly deforms according to Hooke's law, and that the restoring torque (normal reaction force on the meshing teeth) is proportional to the relative rotational displacement.

Fig. 2 shows schematics of the possible modes of gear operation. In 'quiet' operation, the gears remain in contact, and the system resides permanently in regime (a). However in 'noisy' operation, the gears lose contact, and an audible noise is generated by the impact when the gears re-establish contact. There are in fact two broad types of noisy operation.

Starting from regime (a) in Figure 2(a), the gears can lose contact (passing into regime (b)), and then re-establish contact in regime (a) again; this corresponds to X driving Y, occasionally slipping in and out of the freeplay region. Alternatively, the system may include torque reversal (regime (c)); in this situation, X drives Y and Y drives X alternately with periods where the gears are not in contact. Both modes are known as backlash oscillation. We believe that the latter oscillations are the noisiest (certainly torque reversal is highly undesirable), while the former, although not silent, result in quieter operation.

We shall model each shaft with its attached gear and rotor as a single rigid body. This is a simple 'lumped' approach; we do not attempt to model the elastic deformation of individual components, nor do we model the spatial distribution of strain via, for example, Navier equations. In order to derive the equations of motion for the system, we must consider the forces acting on the two shafts, as shown schematically in Fig. 3. We now outline the notation introduced in Fig. 3, which portrays more general ratios than 1:1:

- r_{X} and r_{Y} denote the radii of the pitch circles at which the X and Y gears mesh. In the remainder of this paper we restrict attention to the choice $r_{\mathrm{X}} = r_{\mathrm{Y}}$.
- θ_{X} and θ_{Y} denote the angular displacements of the two gears, with directions chosen so that both coordinates increase in time.
- I_{X} and I_{Y} denote the moments of inertia of the fully assembled shafts.
- c_{X} and c_{Y} are linear damping coefficients. Both the X and Y-shafts suffer resistive torques against the direction of motion, given by $c_{\mathrm{X}}\dot{\theta}_{\mathrm{X}}$ and $c_{\mathrm{Y}}\dot{\theta}_{\mathrm{Y}}$ respectively. The linear damping terms arise from lubrication losses, friction in the seals, and a crude attempt to model the force applied in pumping the gas load.
- The relative rotational displacement is defined generally by $r_{\mathrm{X}}\theta_{\mathrm{X}} - r_{\mathrm{Y}}\theta_{\mathrm{Y}}$. Here, where $r_{\mathrm{X}} = r_{\mathrm{Y}}$, we work with the non-dimensional relative rotational

displacement $\Theta := \theta_{\mathrm{X}} - \theta_{\mathrm{Y}}$.

- The stiffness coefficient k is a measure of the lumped torsional rigidity of the shaft assemblies. Each gear experiences a restoring normal reaction force B, which we suppose for simplicity acts normal to the shafts, and which is dependent on the relative position of the gear teeth (and hence the relative rotational displacement). Here B is a nonlinear backlash function that is made up of three linear components. We have

$$B(\Theta, \beta, k) = \begin{cases} k(\Theta - \beta), & \Theta > \beta, & \text{(X drives Y)} \\ 0, & |\Theta| < \beta, & \text{(freeplay)} \\ k(\Theta + \beta), & \Theta < -\beta. & \text{(Y drives X)} \end{cases} \tag{1}$$

  In practice, of course, nonlinear effects such as lubrication, preloads or bending stiffnesses modify the form of the backlash function, but we take only the simplest approach here.

2.1 Eccentricity

We shall be primarily interested in forcing mechanisms that operate at the gross rotation rate of the machine (or multiples thereof); possible candidates are torque ripple and eccentric mounting of the gears. Eccentric mounting is where the axis of rotation does not coincide with the centre of the gear (note that the entire shaft assembly is balanced so that the centre of mass is at the centre of rotation). Even very small eccentricities can give rise to a sufficiently large forcing to drive noisy operation.

We now describe the mechanism by which eccentricity introduces an oscillatory term into the equation of motion of the gears. The key point to note is that for an eccentrically mounted gear, the coordinate Θ which describes the rotational displacement about the shaft is not the same as the angle which parametrises the pitch circle of the gear, where meshing occurs. Whereas the rate of change of angular momentum should be expressed about the shaft, the relative rotational displacement involved in computing the meshing force should be computed at the pitch circle. We must therefore relate the two angles.

For the case of two circular gears of equal radii, it can be shown that

$$\Theta_{\mathrm{outer}} = \Theta_{\mathrm{shaft}} + \epsilon \cos(2\pi\Omega\tau), \tag{2}$$

where Θ_{outer} and Θ_{shaft} are the relative rotational displacements measured at the outer radii and the shaft respectively. Here Ω is the gross rotational

frequency (assumed constant), and ϵ is an effective eccentricity given by

$$\epsilon = \sqrt{\epsilon_{\rm X}^2 + \epsilon_{\rm Y}^2 - 2\epsilon_{\rm X}\epsilon_{\rm Y}\cos\zeta}, \tag{3}$$

where $\epsilon_{\rm X}$ and $\epsilon_{\rm Y}$ are the non-dimensional eccentricities of the X and Y shafts respectively, and the phase angle ζ describes the relative orientation of the eccentricities.

2.2 Equations of motion

For simplicity, we shall assume for the rest of this paper that the two shafts are identical; namely that the inertias, damping and radii of the X and Y-shafts are equal to I, c and r respectively. We will also neglect torque ripple, and assume that the driving torque $T(\tau)$ is a constant, $\overline{T}$. By applying Newton's second law of motion in angular coordinates, we can derive equations of motion of the two shaft assemblies; namely for the X-shaft we have

$$I\ddot{\theta}_{\rm X} + c\dot{\theta}_{\rm X} + rb(\theta_{\rm X}, \theta_{\rm Y}, \tau) = \overline{T}, \tag{4}$$

and for the Y-shaft assembly, we have

$$I\ddot{\theta}_{\rm Y} + c\dot{\theta}_{\rm Y} - rb(\theta_{\rm X}, \theta_{\rm Y}, \tau) = 0, \tag{5}$$

where $b(\theta_{\rm X}, \theta_{\rm Y}, \tau)$ is the interaction force between the gears given by

$$b(\theta_{\rm X}, \theta_{\rm Y}, \tau) = B(\theta_{\rm X} - \theta_{\rm Y} + e(\tau), \beta, k), \tag{6}$$

where $e(\tau)$ is the oscillatory correction for eccentricity, of magnitude ϵ and frequency $2\pi\Omega$. Here B is the backlash function described by (1).

Note that if the gears are turning at a constant speed then the mean drive must balance with the dissipation. Hence, if we define $\overline{\dot{\theta}_{\rm X}}$, $\overline{\dot{\theta}_{\rm Y}}$ and $\overline{b}$ to be the average values of $\dot{\theta}_{\rm X}$, $\dot{\theta}_{\rm Y}$ and b respectively, we have

$$\frac{c}{I}\overline{\dot{\theta}_{\rm X}} + \frac{r}{I}\overline{b} = \frac{\overline{T}}{I}, \tag{7}$$

$$\frac{c}{I}\overline{\dot{\theta}_{\rm Y}} - \frac{r}{I}\overline{b} = 0. \tag{8}$$

Adding (7) to (8) and assuming the average rotational speed is $\overline{\dot{\theta}_{\rm X}} = \overline{\dot{\theta}_{\rm Y}} = 2\pi\Omega$, we then obtain

$$\overline{T} = 4\pi c\Omega. \tag{9}$$

Now, let $y(\tau) = \theta_{\rm X}(\tau) - \theta_{\rm Y}(\tau) + e(\tau)$ then, from (4) and (5), we obtain

$$\ddot{y} + \frac{c}{I}\dot{y} + \frac{2r}{I}B(y, \beta, k) = \frac{4\pi c\Omega}{I} + \frac{c}{I}\dot{e} + \ddot{e}. \tag{10}$$

For lightly loaded gears, we may neglect the $(c/I)\dot{e}$ term on the right-hand side of (10); the eccentricity and damping are both typically very small so this term is much smaller in magnitude than the other two, and hence we may approximate the forcing in (10) for simplicity by

$$\frac{4\pi c\Omega}{I} + \Omega^2 \epsilon \cos(2\pi\Omega\tau). \tag{11}$$

Thus, if we define a dimensionless time t as $t = \Omega\tau$, denoting differentiation with respect to t by an apostrophe, we can recast (10) as

$$y'' + \frac{c}{I\Omega}y' + \frac{2r}{I\Omega^2}B(y,\beta,k) = \frac{4\pi c}{I\Omega} + \epsilon\cos(2\pi t). \tag{12}$$

Finally, setting the new parameters

$$\delta = \frac{c}{\Omega I}, \quad \kappa = \frac{rk}{\Omega^2 I}, \tag{13}$$

we obtain

$$y'' + \delta y' + 2B(y,\beta,\kappa) = 4\pi\delta + \epsilon\cos(2\pi t), \tag{14}$$

with $B(y,\beta,\kappa)$ as given by (1).

As it stands, our model (14) is a nonlinear second order ordinary differential equation, with the nonlinearity arising from the backlash term B. However, (14) can be split into the three linear regimes of B:

(a) $y > \beta$ (X drives Y)

$$y'' + \delta y' + 2\kappa(y-\beta) = 4\pi\delta + \epsilon\cos(2\pi t), \tag{15}$$

(b) $|y| < \beta$ (freeplay)

$$y'' + \delta y' = 4\pi\delta + \epsilon\cos(2\pi t), \tag{16}$$

(c) $y < -\beta$ (Y drives X)

$$y'' + \delta y' - 2\kappa(y+\beta) = 4\pi\delta + \epsilon\cos(2\pi t). \tag{17}$$

The three equations (15), (16) and (17) are linear ordinary differential equations, which can each be solved explicitly for y using standard techniques. The nonlinearity arises because the motion $y(t)$ will typically not be confined to any one of the regions for all time, but will swap whenever y passes through the values $\pm\beta$.

For typical machines, the stiffness κ is very large, and so we can also think of taking an impacting model of backlash ($\lim_{\kappa\to\infty} B(y,\beta,\kappa)$; see Fig. 5), in which the system evolves only according to (16), with an instantaneous impact condition applied whenever $y = \pm\beta$. In what follows, we will model the contacts in both ways.

Firstly, we will seek a condition for the existence of silent solutions that are confined to the linear stiffness regime $y > \beta$ for all time. We will then focus on various families of periodic rattling solutions, and show their regions of existence and stability in parameter space, comparing the results of the analysis with the piecewise linear (PWL) contact model ($\kappa < \infty$) with those of the impacting model of backlash ($\lim_{\kappa\to\infty}$). We will show that systems with backlash can exhibit both standard bifurcations, as well as bifurcations unique to non-smooth systems (known as discontinuity-induced bifurcations) [19]. We derive two-parameter bifurcation diagrams (including novel codimension-two [20] phenomena) analytically, and validate them through numerical simulations.

3 Permanent contact solution

Geared systems should be designed to operate so that the gear teeth remain in contact for all time, with no rattle. It is straightforward to derive a condition for such a solution to exist. For the gears to remain in contact, the solution must be confined within the phase-space region where $y > \beta$ (see Figure 4) where the system is described by the equation

$$y'' + \delta y' + 2\kappa(y - \beta) = 4\pi\delta + \epsilon\cos(2\pi t), \quad y > \beta. \tag{18}$$

The change of variable $\hat{y} = y - \beta - 2\pi\delta/\kappa$ gives

$$\hat{y}'' + \delta\hat{y}' + 2\kappa\hat{y} = \epsilon\cos(2\pi t), \quad \hat{y} > -\frac{2\pi\delta}{\kappa}. \tag{19}$$

If we assume $u(t) = \cos(2\pi t)$ to be the external input to the dynamical system described by (19), we can derive its transfer function as

$$G(s) = \frac{\mathcal{L}(\hat{y}(t))}{\mathcal{L}(u(t))} = \frac{\epsilon}{s^2 + \delta s + 2\kappa}. \tag{20}$$

where $\mathcal{L}$ is the Laplace transform operator.

Thus neglecting transients, the system response to the sinusoidal forcing input $\cos(2\pi t)$ is a sinusoid centred at $\hat{y} = 0$ with magnitude determined by

$$|G(2\pi\mathrm{i})| = \frac{\epsilon}{\sqrt{(2\kappa - 4\pi^2)^2 + 4\pi^2\delta^2}}. \tag{21}$$

For the permanent linear contact ($\hat{y}(t) > -2\pi\delta/\kappa$ for all t) solution to exist,

we must have $|G(2\pi \mathrm{i})| < 2\pi\delta/\kappa$, namely

$$\epsilon < \frac{2\pi\delta}{\kappa}\sqrt{(2\kappa - 4\pi^2)^2 + 4\pi^2\delta^2}. \tag{22}$$

In the $\kappa \to \infty$ limit of large stiffness, the condition for silent operation reduces to

$$\epsilon < 4\pi\delta. \tag{23}$$

There is a range of anecdotal evidence to suggest that satisfying this bound in real geared systems is a major challenge. However, choosing parameters such that (22) is satisfied is not enough to guarantee silent operation; stable rattling solutions may also coexist, as we shall see in the following sections. Throughout, we suppose that (23) holds so that in particular the RHS of (18) is positive for all time — this assumption simplifies the subsequent analysis considerably.

4 Backlash model and parameter values

The model we have obtained so far is a single degree of freedom system involving a small set of non-dimensional parameters. An important issue is to decide the parameter ranges to be analysed. Motivated by the Roots blower application, the setting on which we will focus is one where the stiffness is very large, while the damping, backlash and eccentricity are very small. We therefore make the simplifying assumption that δ, ϵ and β all have similar (small) magnitudes, i.e.

$$\delta \sim \beta \sim \epsilon. \tag{24}$$

It remains only to choose a scaling for κ. Henceforth, we adopt

$$\kappa \sim \mathcal{O}(1/\delta^2), \tag{25}$$

although we believe that our asymptotics will also work for other similar scalings.

For the purposes of asymptotic expansions, it is convenient to express all parameters in terms of a single small parameter. To this end we may write

$$\beta = \beta_1\delta, \tag{26}$$
$$\epsilon = \epsilon_1\delta, \tag{27}$$

and for the PWL contact model

$$\kappa = \frac{\kappa_1}{\delta^2}, \tag{28}$$

where $\epsilon_1, \beta_1, \kappa_1 \sim \mathcal{O}(1)$.

In what follows, we will examine the existence, stability and bifurcations of periodic rattling solutions of (14) with two different stiffness models, illustrated schematically in Fig. 5. The first is an impacting model, described by a simple coefficient of restitution law, while the second is based on a piecewise linear stiffness law. The advantage of the impacting model is that it is considerably simpler to analyse, and as we shall show, it has equivalent dynamics to the piecewise linear model for large finite κ.

In the impacting model, the parameters that can be varied are δ, ϵ and β. By assumption (23), we need only derive results in the transformed cross-section of parameter space shown in Fig. 6. Since our calculations are analytical rather than numerical, the variation with β will turn out to be clear.

4.1 Impacting contact model

In the systems we consider here, the motion of the gears is mostly free as they are affected by only a small amount of damping. During rattling motion, we expect therefore that the gears are in contact for small periods of time, quickly bouncing back to the region characterised by $y < \beta$, whenever it comes in contact with the backlash boundary. Note that the impacting model, shown in Fig. 5, can be seen as the limit of the piecewise linear one when the stiffness becomes infinitely large, i.e. when $\kappa \to \infty$.

It is shown in [21] that, as $\kappa \to \infty$, it is valid to approximate the contact as a pure impact through a classical coefficient of restitution law. The problem to address is to find the value of the coefficient of restitution. Namely, we assume that whenever $|y| = \beta$, y' changes sign and is multiplied by a constant r, the coefficient of restitution. We estimate r heuristically as detailed below.

The general solution to our differential equation (14) in the contact region $y > \beta$ is given by

$$y(t) = \exp\left(-\frac{\delta t}{2}\right)\left(C_1 \cos\left(t\sqrt{2\kappa - \frac{\delta^2}{4}}\right) + C_2 \sin\left(t\sqrt{2\kappa - \frac{\delta^2}{4}}\right)\right) + \beta + P(t), \tag{29}$$

where C_1 and C_2 are constants of integration and $P(t)$ is the particular solution of our linear equation, given by:

$$P(t) = \frac{2\pi\delta}{\kappa} + \frac{\epsilon}{2(\kappa - 2\pi^2)^2 + 2\pi^2\delta^2}\left((\kappa - 2\pi^2)\cos(2\pi t) + \pi\delta \sin(2\pi t)\right). \tag{30}$$

We can see that $P(t) \sim \mathcal{O}(1/\kappa)$, therefore $\lim_{\kappa\to\infty} P(t) = 0$.

Moreover, when $\kappa \to \infty$, we have

$$\sqrt{2\kappa - \frac{\delta^2}{4}} \sim \sqrt{2\kappa}. \tag{31}$$

Therefore the solution in the limit $\kappa \to \infty$ becomes

$$\lim_{\kappa\to\infty} y(t) = \exp\left(-\frac{\delta t}{2}\right)\left(C_1\cos(\sqrt{2\kappa}t) + C_2\sin(\sqrt{2\kappa}t)\right) + \beta, \tag{32}$$

At the point where we make contact we assume w.l.o.g. that $t = 0$ and $y(0) = \beta$, $y'(0) = v_0 > 0$. Therefore we have

$$\lim_{\kappa\to\infty} y(t) = \frac{1}{2}\exp\left(-\frac{\delta t}{2}\right)\frac{v_0}{\sqrt{2\kappa}}\sin(\sqrt{2\kappa}t) + \beta. \tag{33}$$

We leave contact again when $y(t) = \beta$, i.e. when

$$t = \frac{\pi}{\sqrt{2\kappa}}, \tag{34}$$

which tends to zero as $\kappa \to \infty$. The velocity at this time v_1 is given by

$$v_1 = -v_0 + \mathcal{O}(\delta^2), \tag{35}$$

Therefore to second order in δ the velocity is reversed and hence the coefficient of restitution is unity to good approximation.

4.2 Piecewise linear contact model

As mentioned in the introduction, we are interested in the analysis of solutions (associated to rattling) that can coexist with a perfectly meshed solution, i.e. where $y > \beta$ for all t (sufficiently large). When using the impacting model, we remove the possibility for such a solution to exist (as a trajectory cannot enter the region $|y| > \beta$). Therefore, we also consider a backlash model characterised by the piecewise linear stiffness law described by $B(y, \beta, \kappa)$ as given by (1).

Now, suppose κ is a finite large value satisfying (25). We then have $P(t) \sim \mathcal{O}(\delta^3)$. However, this is not of low enough order to discard and still accurately find the Floquet multipliers of the solutions we will construct. Therefore when dealing with solutions in the piecewise linear contact model case we have to deal with the full general solutions of our differential equation.

Currently, it is not clear in the existing literature to what extent the two modelling approaches yield the same result. An important open problem is

to understand whether the impacting model can be seen as the singular limit of a family of finite stiffness ones. In what follows, we shall take a practical approach, seeking to compare the dynamics predicted by the two models, providing both analytical and numerical evidence for their similarities and differences.

5 Methodology to determine existence and stability of periodic solutions

As a first step, we describe methods to determine analytically the regions of existence and stability of different orbits by using both the impacting and piecewise linear models of the contact force. We introduce an appropriate notation to classify the different possible types of orbits.

5.1 Classification of periodic orbits

For convenience we introduce a notation to identify periodic orbits characterised by different phase-space itineraries. If we let T be the period of the external forcing (note that in our case T has been rescaled to unity), a periodic solution is denoted by $P(m, n^+, n^-)$ where

- m is the periodicity of the solution, in the sense that $y(t) = y(t + mT)$.
- n^+ is the number of times per period the orbit makes contact with the boundary at $y = +\beta$.
- n^- is the number of times per period the orbit makes contact with the boundary at $y = -\beta$.

For example, an orbit of type $P(2, 1, 1)$ is a solution that repeats itself every 2 cycles of the forcing and hits each boundary once per period; see Figure 7 for further examples. We further distinguish between 'in-phase' and 'out-of-phase' solutions. In-phase solutions have their maxima at times close to the times of the maxima of the forcing (i.e. $t = 0, 1, 2, 3 \ldots$), whilst out-of-phase solutions have their maxima close to the times of the forcing minima (i.e. $t = 1/2, 3/2, 5/2, \ldots$).

5.2 Existence of periodic orbits

The system under investigation is described by a piecewise linear differential equation. We can therefore find its solutions analytically in between boundary events that determine changes from one system configuration to another. To

obtain conditions for the existence of a given periodic solution, we then have to 'glue' sections of trajectories belonging to different phase-space regions, by computing accurately the times at which the boundary events occur. It is worth mentioning here that the conditions of existence obtained by following this approach are only necessary. Hence, we will have to check *a posteriori* that the orbit satisfying the conditions is indeed described by the correct itinerary, i.e. the correct sequence of boundary events.

As will be shown later, we obtain a set of implicit transcendental equations of the form $\boldsymbol{f}(\boldsymbol{x}, \boldsymbol{p}) = \boldsymbol{0}$,where $\boldsymbol{p}$ is a vector of parameters;

- $\boldsymbol{p} = [\delta, \beta, \epsilon, \kappa]^{\mathrm{T}}$ with the PWL contact model,
- $\boldsymbol{p} = [\delta, \beta, \epsilon]^{\mathrm{T}}$ with the impacting model,

and $\boldsymbol{x}$ is a vector of unknowns. We will seek approximate solutions of such equations by using appropriate asymptotic expansions. Writing each parameter in terms of the small parameter δ, (26)–(28), we can expand the unknowns $\boldsymbol{x}$ as a series in δ

$$\boldsymbol{x} = \ldots + \boldsymbol{x}_{-1}\delta^{-1} + \boldsymbol{x}_0 + \boldsymbol{x}_1\delta + \ldots, \tag{36}$$

where the terms $\boldsymbol{x}_i \sim \mathcal{O}(1)$, and hence obtain solutions of $\boldsymbol{f}(\boldsymbol{x}, \boldsymbol{p}) = \boldsymbol{0}$ for small δ. It is these solutions which lead to the conditions of existence.

The assumption that the external forcing term is positive, implied by (23), allows us to draw some important information about turning points in the region $|y(t)| < \beta$. At a turning point $y'(t) = 0, |y(t)| < \beta$ we have

$$y'' = 4\pi\delta + \epsilon\cos(2\pi t). \tag{37}$$

The acceleration $y''(t)$ must therefore be positive at such a turning point. Therefore we cannot have a maximum in the region $|y(t)| < \beta$. This allows us safely to ignore some of the constraints on our sections of trajectory. If we have a trajectory starting at $y(t) = -\beta, y'(t) > 0$ then the next boundary hit has to be the boundary $y(t) = \beta$. However, trajectories that start at $y(t) = \beta, y'(t) < 0$ may next hit either the boundary $y(t) = \beta$ or $y(t) = -\beta$.

5.3 Stability of periodic orbits

We have to take special care when investigating the stability of periodic solutions in our system, in particular to account for possible jumps in the Jacobian due to trajectories crossing the boundaries defined by $|y| = \beta$.

For both models of the backlash considered here, we have to investigate how perturbed solutions behave in the differentiable region of phase-space $|y| < \beta$

(Section 5.3.1). When using the piecewise linear contact model, we must also consider the behaviour of the system under perturbations in the differentiable regions $|y| > \beta$ (Sec. 5.3.2). This involves the use of classical Floquet analysis (see e.g. [22]).

At the non-smooth boundaries there may be jumps in the Jacobian matrix of the solution, which must be taken into account. This is only important when the backlash is modelled by an impacting law, as the discontinuity induced by the piecewise linear one is in terms of order higher than linear and therefore we do not need to add any correction. The correction in the impacting case is calculated using the so-called *discontinuity mapping* [23–25].

In conclusion, to determine the overall stability of a given periodic solution, we can multiply the Jacobians associated to small perturbations in each of the phase-space regions visited by the solution of interest with the discontinuity mappings accounting for the occurrence of boundary events.

5.3.1 Stability: freeplay region $|y| < \beta$

We consider a trajectory that enters this region at $t = t_0$ and leaves at $t = t_1$. Thus, if we let $y_1 = y$ and $y_2 = y'$ we have for $t \in (t_0, t_1)$

$$\frac{\mathrm{d}}{\mathrm{d}t}\begin{bmatrix} y_1 \\ y_2 \end{bmatrix} = \begin{bmatrix} y_2 \\ -\delta y_2 + 4\pi\delta + \epsilon\cos(2\pi t) \end{bmatrix}. \tag{38}$$

Let $\boldsymbol{Y}_0$ be the section of trajectory lying in this region. We wish to investigate the effects of a small disturbance $\boldsymbol{z}(t)$ on $\boldsymbol{Y}_0$. Namely, we have

$$\boldsymbol{y}(t) = \boldsymbol{Y}_0(t) + \boldsymbol{z}(t). \tag{39}$$

Substituting this into (38), expanding in a Taylor series about Y_0 and retaining only the linear terms we find

$$\boldsymbol{z}'(t) = A\boldsymbol{z}, \tag{40}$$

where A is the Jacobian of our system (38), given by

$$A = \begin{bmatrix} 0 & 1 \\ 0 & -\delta \end{bmatrix}. \tag{41}$$

(Note that, in general, this matrix is a function of time.)

The two-dimensional linear system (40) has two linearly independent solutions

$\boldsymbol{z}_1$ and $\boldsymbol{z}_2$. We write these as a *fundamental matrix solution*

$$Z(t) = [\boldsymbol{z}_1\ \boldsymbol{z}_2]\,, \tag{42}$$

which satisfies

$$Z' = AZ. \tag{43}$$

This equation describes the evolution of the perturbation between the times t_0 and t_1. In particular, solving (43) for a general initial condition $Z(t_0)$, we find

$$Z(t_1) = \Phi_1(t_1 - t_0)Z(t_0), \tag{44}$$

where

$$\Phi_1(t_1 - t_0) = \begin{bmatrix} 1 & \frac{1}{\delta}(1 - \mathrm{e}^{-\delta(t_1 - t_0)}) \\ 0 & \mathrm{e}^{-\delta(t_1 - t_0)} \end{bmatrix}. \tag{45}$$

The matrix operator Φ_1 can be thought of as the mapping that needs to be applied to the perturbation $Z(t_0)$ at time t_0, when the perturbed trajectory enters into the region $|y| < \beta$. Therefore, if the eigenvalues of Φ_1 are all inside the unit circle, the perturbation would decrease. Note that the determinant of Φ_1 is $\mathrm{e}^{-\delta(t_1 - t_0)}$ and the eigenvalues are 1 and $\mathrm{e}^{-\delta(t_1 - t_0)}$. This means that that there is a contraction in one eigendirection and no contraction or expansion in the other.

To assess the stability of the entire periodic solution of interest we need now to compose the operator describing the stability of the trajectory in the region $|y| < \beta$ with the operators describing the trajectory in the other phase-space regions. As stated above, this varies according to the backlash model being considered. In what follows, we discuss first the case of the piecewise linear model and then the impacting model, showing that in both cases it is possible to obtain appropriate stability conditions.

5.3.2 Stability: piecewise linear contact model ($|y| > \beta$)

If backlash is modelled by a piecewise linear contact law, then the trajectory will have segments lying in the regions $|y| > \beta$. To investigate the effects of small perturbations on these sections of trajectory, we can use the same approach presented in Sec. 5.3.1. Here the fundamental matrix solution satisfies

$$Z' = \begin{bmatrix} 0 & 1 \\ -2\kappa & -\delta \end{bmatrix} Z, \tag{46}$$

and we can solve to get $Z(t_1) = \Phi_2(t_1 - t_0)Z(t_0)$, where

$$\Phi_2(t_1 - t_0) = \begin{bmatrix} \frac{\lambda_2}{2\kappa} & \frac{\lambda_1}{2\kappa} \\ 1 & 1 \end{bmatrix} \begin{bmatrix} \mathrm{e}^{\lambda_1(t_1-t_0)} & 0 \\ 0 & \mathrm{e}^{\lambda_2(t_1-t_0)} \end{bmatrix} \begin{bmatrix} \frac{\lambda_2}{2\kappa} & \frac{\lambda_1}{2\kappa} \\ 1 & 1 \end{bmatrix}^{-1}, \tag{47}$$

with

$$\lambda_1 = -\frac{\delta}{2} + \sqrt{\frac{\delta^2}{4} - 2\kappa}, \qquad \lambda_2 = -\frac{\delta}{2} - \sqrt{\frac{\delta^2}{4} - 2\kappa}. \tag{48}$$

The determinant of $\Phi_2(t)$ is then given by $\mathrm{e}^{(\lambda_1+\lambda_2)t} = e^{-\delta t}$, and the eigenvalues are $e^{\lambda_1 t}$ and $\mathrm{e}^{\lambda_2 t}$. As we have assumed that $\kappa \gg \delta$, these eigenvalues will always be within the unit circle and perturbations will contract in these regions.

5.3.3 Stability: impacting contact model

To investigate the stability of orbits when an impacting model is used to describe the backlash in the system, we use the method based on so-called discontinuity mappings; for further details see [26].

Use of the discontinuity mapping allows us to correct for changes in the Jacobian matrix of the solution at a boundary event. It is derived by considering perturbations from a reference solution. The Jacobian of the complete orbit is derived by multiplying the Jacobians of the smooth sections by the derivative of the discontinuity mapping.

Suppose that the trajectory hits the impacting boundary at the point $\boldsymbol{y}_{\text{in}} = [y_{\text{in}}, y'_{\text{in}}]^{\text{T}}$ at time t_{in}, and is mapped under the coefficient of restitution law to the point $\boldsymbol{y}_{\text{out}} = [y_{\text{out}}, y'_{\text{out}}]^{\text{T}}$.

As detailed in [26], the matrix to correct the Jacobian of the solution is given by

$$D(t_{\text{in}}, \boldsymbol{y}_{\text{in}}) = \boldsymbol{g}_{\boldsymbol{y}}(\boldsymbol{y}_{\text{in}}) + \frac{(\boldsymbol{f}_{\text{out}} - \boldsymbol{g}_{\boldsymbol{y}}(\boldsymbol{y}_{\text{in}})\boldsymbol{f}_{\text{in}})h_{\boldsymbol{y}}(\boldsymbol{y}_{\text{in}})}{h_{\boldsymbol{y}}(\boldsymbol{y}_{\text{in}})\boldsymbol{f}_{\text{in}}}, \tag{49}$$

where

- $\boldsymbol{g}(\boldsymbol{y})$ is the mapping that is applied to the flow at the discontinuity boundary, in our case

$$\boldsymbol{g}(\boldsymbol{y}) = \begin{bmatrix} 1 & 0 \\ 0 & -1 \end{bmatrix} \boldsymbol{y}, \tag{50}$$

  such that $\boldsymbol{y}_{\text{out}} = \boldsymbol{g}(\boldsymbol{y}_{\text{in}})$.
- $h(\boldsymbol{y})$ is the scalar function that defines the boundary between the areas of

phase-space. In our case we have two,

$$h_{\pm}(\boldsymbol{y}) = \begin{bmatrix} 1 & 0 \end{bmatrix} \boldsymbol{y} \pm \beta. \tag{51}$$

- $\boldsymbol{f}_{\text{in}}$ and $\boldsymbol{f}_{\text{out}}$ are the values of the vector field at $\boldsymbol{y}_{\text{in}}$ and $\boldsymbol{y}_{\text{out}}$ respectively.

The correction matrix is therefore given by

$$D(t_{\text{in}}, \boldsymbol{y}_{\text{in}}) = \begin{bmatrix} -1 & 0 \\ \dfrac{8\pi\delta}{y'_{\text{in}}} + \dfrac{2\epsilon}{y'_{\text{in}}} \cos(2\pi t_{\text{in}}) & -1 \end{bmatrix}. \tag{52}$$

Now we show how the results obtained for different phase-space regions can be combined to investigate the stability of a particular solution. Namely, we need to multiply the matrices Φ_1, Φ_2 and D in the appropriate order to find the Floquet multipliers of the whole solution. We illustrate the procedure by investigating in detail the existence and stability of the two simplest types of 'noisy' periodic orbit: those that have one contact per period with the boundary at $y = \beta$, of type $P(m, 1, 0)$, and those with one contact per period with each boundary $y = \pm\beta$, of class $P(m, 1, 1)$. As these are the simplest periodic orbits, we expect them to have larger basins of attraction than orbits with many contacts per period.

6 $P(m, 1, 0)$ periodic orbits

We use the methods presented in Sec. 5 to investigate solutions that contact only the boundary $y = \beta$ once per period, i.e. of type $P(m, 1, 0)$. In Sec. 6.1, we investigate these solutions when the impacting contact backlash model is considered (see Figure 8). Then, in Sec. 6.2 we investigate the same type of solutions but with the piecewise linear contact model (see Fig. 11). We show that these have the same leading order behaviour, and present our findings on two-parameter bifurcation diagrams, shown in Figs. 9 and 10.

6.1 Impacting contact model

6.1.1 Existence

Here we should point out that we can only have $P(m, 1, 0)$ solutions that contact the boundary at $y = \beta$. We cannot have solutions that only impact the boundary $y(t) = -\beta$, as shown in Sec. 5.2.

Our first step is to construct the unknown part of our solutions. With reference to Fig. 8, we construct the solution such that immediately after impact

$$y(\phi) = \beta, \tag{53}$$
$$y'(\phi) = -v, \tag{54}$$

for some unknown initial time ϕ and velocity $-v$. The periodicity conditions then imply that immediately before the next impact

$$y(m+\phi) = \beta, \tag{55}$$
$$y'(m+\phi) = v. \tag{56}$$

Solving these equations without resorting to expansions, after a few algebraic manipulations we obtain

$$\beta = 4\pi\phi - \frac{\epsilon}{2\pi\sqrt{\delta^2+4\pi^2}}\cos\left(2\pi\phi + \arctan\left(\frac{\delta}{2\pi}\right)\right) + c_1 + c_2\,\mathrm{e}^{-\delta\phi}, \tag{57}$$

$$-v = 4\pi + \frac{\epsilon}{\sqrt{\delta^2+4\pi^2}}\sin\left(2\pi\phi + \arctan\left(\frac{\delta}{2\pi}\right)\right) - c_2\delta\,\mathrm{e}^{-\delta\phi}, \tag{58}$$

$$\beta = 4\pi(\phi+m) - \frac{\epsilon}{2\pi\sqrt{\delta^2+4\pi^2}}\cos\left(2\pi\phi + \arctan\left(\frac{\delta}{2\pi}\right)\right) + c_1 + c_2\,\mathrm{e}^{-\delta(\phi+m)}, \tag{59}$$

$$v = 4\pi + \frac{\epsilon}{\sqrt{\delta^2+4\pi^2}}\sin\left(2\pi\phi + \arctan\left(\frac{\delta}{2\pi}\right)\right) - c_2\delta\,\mathrm{e}^{-\delta(\phi+m)}, \tag{60}$$

where c_1 and c_2 are the undetermined integration constants. From (59) and (57), we have

$$0 = -4\pi m + c_2\,\mathrm{e}^{-\delta\phi}(1-\mathrm{e}^{-\delta m}), \tag{61}$$

and, using (60) and (58), we obtain

$$-2v = -c_2\delta\,\mathrm{e}^{-\delta\phi}(1-\mathrm{e}^{-\delta m}). \tag{62}$$

Hence we find that

$$v = 2\pi\delta m, \tag{63}$$
$$c_2 = \frac{4\pi m\,\mathrm{e}^{\delta\phi}}{1-\mathrm{e}^{-\delta m}}. \tag{64}$$

Substituting these values for v and c_2 into (60) and solving for ϕ, we have

$$\phi = \frac{1}{2\pi}\left(\arcsin\left(\frac{\sqrt{\delta^2+4\pi^2}}{\epsilon}\left(\frac{4\pi m\delta\,\mathrm{e}^{-\delta m}}{1-\mathrm{e}^{-\delta m}} + 2\pi\delta m - 4\pi\right)\right) - \arctan\left(\frac{\delta}{2\pi}\right)\right). \tag{65}$$

There are two admissible solutions to (65). We can expand these solutions in terms of our small parameters,

$$\phi = \begin{cases} \dfrac{m^2\pi\delta^2}{3\epsilon} - \dfrac{\delta}{4\pi^2} + \mathcal{O}(\delta^3) & : \text{in-phase solution,} \\ \dfrac{1}{2} - \dfrac{m^2\pi\delta^2}{3\epsilon} - \dfrac{\delta}{4\pi^2} + \mathcal{O}(\delta^3) & : \text{out-of-phase solution.} \end{cases} \tag{66}$$

Note that these solutions cannot exist if the argument of the arcsin function in (65) becomes greater than one. Thus, expanding the argument in terms of our small parameters δ and ϵ, we find

$$\frac{\sqrt{\delta^2 + 4\pi^2}}{\epsilon}\left(\frac{4m\pi\delta\,\mathrm{e}^{-m\delta}}{1-\mathrm{e}^{-m\delta}} + 2m\pi\delta - 4\pi\right) = \frac{2m^2\pi^2\delta^2}{3\epsilon} + \mathcal{O}(\delta^2). \tag{67}$$

Hence, for this to be less than one we require that, to leading order,

$$\epsilon > \frac{2\pi^2 m^2\delta^2}{3} + \mathcal{O}(\delta^3). \tag{68}$$

We also must consider whether our trajectory will have the correct itinerary, i.e. that it will not hit the boundary at $y = -\beta$. To show this, we must find the minimum displacement, and to do this we must again resort to approximate methods. To find the minimum displacement we first find the point at which the velocity is zero, i.e. $\hat{t}$ such that $y'(\hat{t}) = 0$. We try a power series approximation

$$\hat{t} = \phi + \frac{m}{2} + \hat{t}_0 + \hat{t}_1\delta + \hat{t}_2\delta^2 + \ldots, \tag{69}$$

and solve for the coefficients $\hat{t}_i$ by comparing terms of $\mathcal{O}(\delta^k)$ in turn. We then substitute this series expression for $\hat{t}$ into our ODE solution $y(t)$, and expand this as a series as well to find the minimum displacement of the candidate periodic orbit $\hat{y} = y(\hat{t})$. For existence of the periodic orbit, we must satisfy $\hat{y} > -\beta$. After algebraic manipulation, we find that, for the in-phase solution ($\phi = \mathcal{O}(\delta)$) not to contact the lower boundary we require

$$\beta > \begin{cases} \dfrac{m^2\pi\delta}{4} + \dfrac{\epsilon}{4\pi^2} - \mathcal{O}(\delta^2) & : m \text{ odd,} \\ \dfrac{m^2\pi\delta}{4} + \mathcal{O}(\delta^2) & : m \text{ even,} \end{cases} \tag{70}$$

and for the out-of-phase solution ($\phi = \frac{1}{2} + \mathcal{O}(\delta)$) not to contact the lower

boundary we require

$$\beta > \begin{cases} \dfrac{m^2\pi\delta}{4} + \dfrac{\epsilon}{4\pi^2} + \mathcal{O}(\delta^2) & : m \text{ odd}, \\ \dfrac{m^2\pi\delta}{4} + \mathcal{O}(\delta^2) & : m \text{ even}. \end{cases} \tag{71}$$

6.1.2 Stability

We can construct our stability conditions using the techniques described in Secs. 5.2 and 5.3. We consider the eigenvalues of the matrix A_1 defined by $A_1 = \Phi_1(m)D(\phi + m, 2\pi m\delta)$,

$$A_1 = \begin{bmatrix} -1 & \frac{1}{\delta}(\mathrm{e}^{-\delta m} - 1) \\ \frac{4}{m} + \frac{\epsilon}{\pi m\delta}\cos(2\pi\phi) & -\frac{1}{\delta}(\mathrm{e}^{-\delta m} - 1)\left(\frac{4}{m} + \frac{\epsilon}{\pi m\delta}\cos(2\pi\phi)\right) - \mathrm{e}^{-\delta m} \end{bmatrix}, \tag{72}$$

where ϕ is defined by (65).

The eigenvalues of this matrix are the Floquet multipliers of the orbit. For stability these multipliers must be within the unit circle. The bifurcations that may occur as these eigenvalues cross the unit circle are considered in the next section.

We consider the stability of the in-phase and out-of-phase solutions we have found corresponding to the two values of ϕ from (65). For the in-phase solution ($\phi = \mathcal{O}(\delta)$) we find the leading order term of the Floquet multipliers to be

$$\lambda_{1,2} = 1 + \frac{\epsilon}{2\pi\delta} \pm \frac{1}{2\pi\delta}\sqrt{\epsilon(\epsilon + 4\pi\delta)} + \mathcal{O}(\delta), \tag{73}$$

of which one is outside the unit circle for $\epsilon < 4\pi\delta$. For the out-of-phase ($\phi = \frac{1}{2} + \mathcal{O}(\delta)$) solution the Floquet multipliers are

$$\lambda_{1,2} = \left(1 - \frac{m\delta}{2}\right) f_{1,2} + \mathcal{O}(\delta^2), \tag{74}$$

where

$$f_{1,2} = 1 - \frac{\epsilon}{2\pi\delta} \pm \frac{\mathrm{i}}{2\pi\delta}\sqrt{\epsilon(4\pi\delta - \epsilon)}. \tag{75}$$

It is clear that $|f_{1,2}| = 1$, therefore $|\lambda_{1,2}| \approx 1 - m\delta/2$ and this solution is thus stable for $\epsilon < 4\pi\delta$ and $\epsilon \sim \delta$. We consider in more detail how stability can change in the next section.

6.1.3 Bifurcations

Using the results obtained so far on the existence and stability of orbits of type $P(m, 1, 0)$ we can now attempt to investigate the bifurcations that such solutions can undergo under parameter variations.

We first consider (classical) bifurcations where we will have a Floquet multiplier on the unit circle. We denote our two Floquet multipliers as λ_1 and λ_2. There are three possibilities for a bifurcation of this type;

(1) Complex conjugate Floquet multipliers on the unit circle: $\lambda_{1,2} = \mathrm{e}^{\pm \mathrm{i}\theta}$. This cannot occur for $\delta > 0$ as we require $\lambda_1\lambda_2 = 1 = \mathrm{e}^{-\delta m}$ (product of the eigenvalues of A_1 is $\det(A_1)$). This implies that there are no secondary Hopf or Neimark bifurcations in our region of interest.

(2) A Floquet multiplier on the unit circle on the negative real axis: $\lambda_1 = -1$ (and therefore $\lambda_2 = -\mathrm{e}^{-\delta m}$). We can then use the fact that $\mathrm{tr}(A_1) = \lambda_1 + \lambda_2$, giving

$$-1 - \frac{1}{\delta}(\mathrm{e}^{-\delta m} - 1)\left(\frac{4}{m} + \frac{\epsilon}{\pi m \delta}\cos(2\pi\phi)\right) + \mathrm{e}^{-\delta m} = -1 - \mathrm{e}^{-\delta m}, \quad (76)$$

which reduces to the condition

$$\cos(2\pi\phi) = -\frac{4\pi\delta}{\epsilon}. \quad (77)$$

This equation can only have solutions for $\epsilon > 4\pi\delta$, i.e., outside our region of interest. A Floquet multiplier at -1 is the condition for a period-doubling bifurcation. Therefore we can have no period-doubling here.

(3) A Floquet multiplier on the unit circle on the positive real axis: $\lambda_1 = +1$ (and therefore $\lambda_2 = \mathrm{e}^{-\delta m}$). Again we use the $\mathrm{tr}(A_1) = \lambda_1 + \lambda_2$ condition to find

$$\cos(2\pi\phi) = -\frac{2\pi\delta(\delta m - 2 + \mathrm{e}^{-\delta m}(\delta m + 2))}{\epsilon(\mathrm{e}^{-\delta m} - 1)}. \quad (78)$$

We can substitute expression (65) for ϕ into this to find the location of this bifurcation in the $\epsilon - \delta$ plane. To leading order the bifurcation line is

$$\epsilon = \frac{2\pi^2 m^2 \delta^2}{3} + \mathcal{O}(\delta^4). \quad (79)$$

An eigenvalue at $+1$ implies that we are at a transcritical, cyclic fold or symmetry-breaking bifurcation. Our solution is not symmetric so we can eliminate symmetry-breaking. Our solutions (in this form) cannot exist past the bifurcation point (see (68)) so we cannot have a transcritical bifurcation. Therefore we have a cyclic-fold bifurcation, where unstable and stable solutions meet and disappear.

In addition to the classical bifurcations highlighted above, backlash oscillators

can also undergo so-called discontinuity induced bifurcations [19,20] associated to tangential intersections of the system trajectory with the backlash boundaries defined by $|y| = \beta$, called grazings. The $P(m, 1, 0)$ orbits can only become tangential to the boundary at $y = -\beta$. It is clear that the locus of the grazing bifurcation is the same as the locus of the condition for the existence derived in Section 6.1.1, conditions (70) and (71).

We present these findings on our two-parameter bifurcation diagrams Figures 9 and 10. These figures contain the conditions of existence that correspond to grazing bifurcations and also the changes in stability that correspond to the classical bifurcations described above. We see a plethora of stable impacting solutions, all of which coexist with the silent permanent contact solution. Provided that $4\pi\delta - \epsilon < 16\beta$, as we increase ϵ from zero while keeping $4\pi\delta - \epsilon$ constant (following the dash/dotted lines in Figs. 9 and 10), we first (at $\epsilon = 2\pi^3 m^2 \delta^2/3$) see a cyclic fold bifurcation that simulatanously gives birth to a pair of solutions that hit $y = \beta$ once per period (m), one stable and one unstable. Increasing ϵ by an order of magnitude then destroys the solutions through grazing bifurcations: in the case of odd m, the stable solution grazes first (at $\epsilon = 4\pi^2\beta - \pi^3 m^2 \delta$), followed by unstable one (at $\epsilon = \pi^3 m^2 \delta - 4\pi^2\beta$); while in the case of odd m, both graze simultaneously (at $\delta = 4\beta/(m^2\pi^2)$).

Thus according to this model, there are infinitely many stable rattling solutions coexisting with the silent permanent contact solution, unless one reduces ϵ to $\mathcal{O}(\delta^2)$. However, in real machine design, other factors that have been omitted from our model, such as lubrication, may invalidate this conclusion. As we might expect, increasing damping, whilst similarly reducing the oscillatory forcing and tightening the backlash, will destroy the rattling solutions. We now turn our attention to the effect of the large finite (rather than infinite) torsional stiffness κ.

6.2 Piecewise linear contact model

We now move to the analysis of periodic solutions of type $P(m, 1, 0)$ when modelling the backlash with a piecewise linear contact characteristic (see Fig. 11). We will outline how it may be shown that the dynamics in the $\kappa \to \infty$ limit are the same as those derived with the impacting contact model.

6.2.1 Existence

We again use the method presented in Section 5.2. When the piecewise linear model is used, the orbit of interest has the form sketched in Figure 11.

We write our parameters in terms of the single small parameter δ (see Sec. 4),

$$\boldsymbol{p} = \begin{bmatrix} \delta \\ \epsilon \\ \beta \\ \kappa \end{bmatrix} = \begin{bmatrix} \delta \\ \epsilon_1\delta \\ \beta_1\delta \\ \kappa_1/\delta^2 \end{bmatrix}. \tag{80}$$

We have the unknowns $\mathbf{x} = [v_a, v_b, \phi, \sigma]^T$ which we write as a series in δ

$$\boldsymbol{x} = \begin{bmatrix} v_{a0} \\ v_{b0} \\ \phi_0 \\ \sigma_0 \end{bmatrix} + \begin{bmatrix} v_{a1} \\ v_{b1} \\ \phi_1 \\ \sigma_1 \end{bmatrix} \delta + \begin{bmatrix} v_{a2} \\ v_{b2} \\ \phi_2 \\ \sigma_2 \end{bmatrix} \delta^2 + \ldots, \tag{81}$$

giving us a set of four equations to solve. These are the matching conditions on each section of the trajectory, 'gluing' each section to the next. Each is derived from the four equations from the solutions of our linear ODEs (15) and (16), for displacement and velocity. The first equations are from the solution of the ODE for $y > \beta$,

$$y'' + \delta y' + 2\kappa(y - \beta) = 4\pi\delta + \epsilon\cos(2\pi t), \tag{82}$$

with initial conditions $y(\phi) = \beta$, $y'(\phi) = v_a$. We then have two matching conditions to glue the trajectory segments together at time $t = \phi + \sigma$, namely

$$y(\phi + \sigma) = \beta, \tag{83}$$
$$y'(\phi + \sigma) = -v_b. \tag{84}$$

In full these equations are

$$a_1\,\mathrm{e}^{\lambda_1(\phi+\sigma)} + a_2\,\mathrm{e}^{\lambda_2(\phi+\sigma)} + a_3\cos(2\pi(\phi+\sigma)) + a_4\sin(2\pi(\phi+\sigma)) + \frac{4\pi\delta}{2\kappa} = 0, \tag{85}$$

and

$$\lambda_1 a_1\,\mathrm{e}^{\lambda_1(\phi+\sigma)} + \lambda_2 a_2\,\mathrm{e}^{\lambda_2(\phi+\sigma)} - 2\pi a_3\sin(2\pi(\phi+\sigma)) + 2\pi a_4\cos(2\pi(\phi+\sigma)) + v_b = 0, \tag{86}$$

where

$$\lambda_1 = \frac{-\delta + \mathrm{i}\sqrt{8\kappa - \delta^2}}{2}, \lambda_2 = \frac{-\delta - \mathrm{i}\sqrt{8\kappa - \delta^2}}{2}, \tag{87}$$

$$a_1 = \frac{\mathrm{e}^{\lambda_1 \phi}}{\lambda_1 - \lambda_2} \left((\lambda_2 a_3 - 2\pi a_4) \cos(2\pi\phi) + (2\pi a_3 + \lambda_2 a_4) \sin(2\pi\phi) - \beta\lambda_2 - v_b \right), \tag{88}$$

$$a_2 = \frac{\mathrm{e}^{\lambda_2 \phi}}{\lambda_1 - \lambda_2} \left((-\lambda_1 a_3 + 2\pi a_4) \cos(2\pi\phi) - (2\pi a_3 + \lambda_1 a_4) \sin(2\pi\phi) + \beta\lambda_1 + v_b \right), \tag{89}$$

$$a_3 = \frac{\epsilon(2\pi^2 + \kappa)}{2(4\pi^4 + 4\pi^2\kappa + \pi^2\delta^2 + \kappa^2)}, \tag{90}$$

$$a_4 = \frac{\pi\epsilon\delta}{2(4\pi^4 + 4\pi^2\kappa + \pi^2\delta^2 + \kappa^2)}. \tag{91}$$

Note that the expressions above are lengthy but straightforward to find; for convenience and accuracy they were derived using the algebraic software package MAPLE [27]. For the sake of brevity, we will not report explicitly all the formulas derived in this way except when it is strictly necessary for the understanding of the methodology.

A similar technique generates the second pair of equations: first the ODE in the freeplay region (16) is solved with initial conditions $y(\phi + \sigma) = \beta$, $y'(\phi + \sigma) = -v_b$, and then we apply the matching conditions

$$y(\phi + m) = \beta, \tag{92}$$

$$y'(\phi + m) = v_a. \tag{93}$$

The four equations (83), (84), (92) and (93) now form a system $\boldsymbol{f}(\boldsymbol{x}, \boldsymbol{p}) = \boldsymbol{0}$ for the unknowns $\boldsymbol{x} = (\phi, \sigma, v_a, v_b)^{\mathrm{T}}$. We substitute (80) and (81) (with the additional assumption that, to leading order, the trajectory in the region $y > \beta$ is a sinusoid, which implies that $\sigma = \pi/\sqrt{2\kappa} + \sigma_2\delta^2$) and expand in terms of our remaining small parameter δ. This enables us to find solutions for our sets of coefficients in turn.

The coefficient of δ^0 in the expansion of $\boldsymbol{f}(\boldsymbol{x}, \boldsymbol{p})$ is

$$\begin{bmatrix} 0 \\ v_{b0} - v_{a0} \\ -m v_{b0} \\ -v_{b0} - v_{a0} \end{bmatrix} = \boldsymbol{0}, \tag{94}$$

which gives us $v_{a0} = v_{b0} = 0$. Now if we consider the coefficients of δ from the

expansion we have

$$\begin{bmatrix} 0 \\ v_{b1} - v_{a1} \\ \frac{m}{2\pi}\left(4m\pi^2 - 2\pi v_{b1} + \epsilon_1 \sin(2\pi\phi_0)\right) \\ 4m\pi - v_{a1} - v_{b1} \end{bmatrix} \delta = \mathbf{0}, \tag{95}$$

from which we obtain $v_{a1} = v_{b1} = 2\pi m$, and hence that $\phi_0 \in \{0, 1/2\}$. We continue in a similar manner by solving the coefficients of δ^2 and δ^3 to find that to $\mathcal{O}(\delta^3)$ we have, for the in-phase solution $\phi_0 = 0$,

$$v_a = 2\pi m\delta - \frac{\pi(4\pi\delta + \epsilon)}{2\sqrt{2\kappa}} + \mathcal{O}(\delta^3), \tag{96}$$

$$v_b = 2\pi m\delta - \frac{\pi(4\pi\delta + \epsilon)}{2\sqrt{2\kappa}} + \mathcal{O}(\delta^3), \tag{97}$$

$$\phi = \left(-\frac{\pi}{2\sqrt{2\kappa}} + \frac{\pi m^2\delta^2}{3\epsilon} - \frac{\delta}{4\pi^2}\right) + \left(-\frac{\pi^2 m\delta^2}{2\epsilon\sqrt{2\kappa}} - \frac{1}{m\kappa} - \frac{\epsilon}{4\pi m\kappa\delta}\right) + \mathcal{O}(\delta^3), \tag{98}$$

$$\sigma = \frac{\pi}{\sqrt{2\kappa}} + \frac{4\pi\delta + \epsilon}{2\pi m\kappa\delta} + \mathcal{O}(\delta^3), \tag{99}$$

and for the out-of-phase solution $\phi_0 = 1/2$,

$$v_a = 2\pi m\delta - \frac{\pi(4\pi\delta - \epsilon)}{2\sqrt{2\kappa}} + \mathcal{O}(\delta^3), \tag{100}$$

$$v_b = 2\pi m\delta - \frac{\pi(4\pi\delta - \epsilon)}{2\sqrt{2\kappa}} + \mathcal{O}(\delta^3), \tag{101}$$

$$\phi = \frac{1}{2} + \left(-\frac{\pi}{2\sqrt{2\kappa}} - \frac{\pi m^2\delta^2}{3\epsilon} - \frac{\delta}{4\pi^2}\right) + \left(\frac{\pi^2 m\delta^2}{2\epsilon\sqrt{2\kappa}} - \frac{1}{m\kappa} + \frac{\epsilon}{4\pi m\kappa\delta}\right) + \mathcal{O}(\delta^3), \tag{102}$$

$$\sigma = \frac{\pi}{\sqrt{2\kappa}} + \frac{4\pi\delta - \epsilon}{2\pi m\kappa\delta} + \mathcal{O}(\delta^3). \tag{103}$$

Examining these expressions leads to the conclusion that they are identical, to leading order, to the corresponding quantities obtained using the impacting contact model. Firstly,

$$v_a - v_b = \mathcal{O}(\delta^3), \tag{104}$$

for both the in-phase and out-of-phase solutions; so to $\mathcal{O}(\delta^3)$ the impacting model with coefficient of restitution equal to one is appropriate. Furthermore, as $\kappa \to \infty$,

$$v_a, v_b \to 2\pi\delta m = v^{\text{imp}}, \tag{105}$$

where v^{imp} is the impact velocity predicted by the impacting contact model (63).

Moreover, the impact times predicted by the two models also match; the 'mid-impact' time $\phi+\sigma/2$ is equal, to order δ^2, to that given by the impacting model, ϕ^{imp} (66), for both the in- and out-of-phase solutions:

$$\phi + \frac{\sigma}{2} = \begin{cases} \left(\dfrac{\pi m^2\delta^2}{3\epsilon} - \dfrac{\delta}{4\pi^2}\right) + \dfrac{\pi^2 m\delta^2}{2\epsilon\sqrt{2\kappa}} + \mathcal{O}(\delta^3) & : \text{in-phase solution,} \\ \dfrac{1}{2} - \left(\dfrac{\pi m^2\delta^2}{3\epsilon} - \dfrac{\delta}{4\pi^2}\right) - \dfrac{\pi^2 m\delta^2}{2\epsilon\sqrt{2\kappa}} + \mathcal{O}(\delta^3) & : \text{out-of-phase solution,} \end{cases} \tag{106}$$

$$= \phi^{\text{imp}} + \mathcal{O}(\delta^2). \tag{107}$$

Additionally, as $\kappa \to \infty$,

$$\sigma \to 0, \tag{108}$$

as we might expect.

Thus the necessary conditions for the existence of $P(m, 1, 0)$ periodic orbits in the impacting and piecewise linear contact models are identical, to leading order, as are the solutions themselves. We now have to check *a posteriori* whether the solution has the correct itinerary, that is whether each of the trajectory sections remain in the assumed region of phase-space; namely $y(t) > -\beta$. It may be shown [7] that the condition for this to hold is again the same to leading order as that found with the impacting contact model.

6.2.2 Stability

Here the stability is given by the eigenvalues of the matrix $A_2 = \Phi_1(m - \sigma)\Phi_2(\sigma)$. Finding expansions for the eigenvalues is cumbersome; upon numerical investigation of the formula for the eigenvalues we can show that, as in the impacting case, we have a stable out-of-phase solution and an unstable in-phase solution. The locations of changes in stability are now summarised.

6.2.3 Bifurcations

We have grazing bifurcations whose locus is defined by the conditions of existence derived in Sec. 6.2.1. Here we also consider the possible types of classical bifurcations:

(1) Complex conjugate Floquet multipliers on the unit circle. Again this is not possible as the determinant of our matrix A_2 is $\mathrm{e}^{-\delta m}$.

(2) A Floquet multiplier on the negative real axis at -1. We use our condition on $\mathrm{tr}(A_2) = \lambda_1 + \lambda_2$, expand in terms of δ and ϵ and find that this is only satisfied if $\epsilon = 4\pi\delta$; the boundary of our region of interest.
(3) A Floquet multiplier on the positive real axis at $+1$. With the assumption $\epsilon \sim \delta$ there is no solution to our trace condition. However, as we found the condition for $\epsilon \sim \delta^2$ in the impacting contact model case we try that here. Indeed we find that the leading order terms for the contact time is

$$\phi = \frac{1}{2\pi} \arcsin\left(\frac{2m^2\pi^2\delta^2}{3\epsilon}\right), \tag{109}$$

which can only have a solution for

$$\epsilon > \frac{2m^2\pi^2\delta^2}{3}, \tag{110}$$

which is the same as the condition with the impacting contact model.

We have therefore shown that, to leading order in the small parameter δ, the piecewise linear finite stiffness model of backlash produces the same bifurcations, both standard and nonstandard, as the impacting model, in the case of $P(m, 1, 0)$ periodic orbits. We now turn our attention to the more complicated family of orbits, those with impacts on both sides of the lash.

7 $P(m, 1, 1)$ periodic orbits

We shall now consider periodic orbits in which the gears enter contact on both sides of the backlash region. From an application point of view, these are potential candidates for bad N&V problems; certainly torque reversal (contact with the boundary $y = -\beta$) is highly undesirable. The simplest solutions of this type are periodic orbits that have only one contact on each side of the lash per period; labelled as $P(m, 1, 1)$ solutions in our notation. As before we consider solutions for the cases of impacting and PWL contact models. We show that both models again exhibit the same bifurcation behaviour to leading order, illustrated graphically in the two-parameter bifurcation diagrams shown in Figs. 13 and 14.

7.1 Impacting contact model

We first consider $P(m, 1, 1)$ solutions with the impacting contact model. The trajectory $y(t)$ is made up of two smooth segments which we label y_a and y_b,

defined by

$$y(t) = \begin{cases} y_a(t) & \phi < t < \psi, \\ y_b(t) & \psi < t < \phi + m, \end{cases} \tag{111}$$

and sketched in Fig. 12.

7.1.1 Existence

To compute the existence conditions for a $P(m, 1, 1)$ orbit, we can solve the ODE in the freeplay region (16) using the initial conditions

$$y_a(\phi) = \beta, \tag{112}$$
$$y_a'(\phi) = -v_1, \tag{113}$$
$$y_b(\psi) = -\beta, \tag{114}$$
$$y_b'(\psi) = v_2, \tag{115}$$

where $v_1 > 0, v_2 > 0$. We then apply our matching conditions for the contacts at $t = \phi$ and $t = \psi$ to get four equations to solve,

$$\boldsymbol{f}(\boldsymbol{x}, \boldsymbol{p}) = \begin{bmatrix} y_a(\psi) \\ y_a'(\psi) \\ y_b(m + \phi) \\ y_b'(m + \phi) \end{bmatrix} = \begin{bmatrix} -\beta \\ -v_2 \\ \beta \\ v_1 \end{bmatrix} \tag{116}$$

for the four unknowns $\boldsymbol{x} = [\phi, \psi, v_1, v_2]^{\mathrm{T}}$.

We carry out expansions as described in Sec. 5.2, to find a power series in δ for each unknown. We again find four cases corresponding to in-phase / out-of-phase and m odd / even. The leading order terms are as follows:

(1) In-phase solution, m odd:

$$v_1 = m\pi\delta + \frac{4\beta}{m} + \frac{\epsilon}{m\pi^2}, \tag{117}$$
$$v_2 = -m\pi\delta + \frac{4\beta}{m} + \frac{\epsilon}{m\pi^2}, \tag{118}$$
$$\phi = \frac{\beta\delta}{\epsilon} - \frac{m^4\pi^3\delta^2(4\pi\delta - \epsilon)}{12\epsilon((m^2\pi^2 - 4)\epsilon - 16\pi^2\beta)}, \tag{119}$$
$$\psi = \frac{m}{2} + \frac{\beta\delta}{\epsilon} - \frac{m^4\pi^3\delta^2(4\pi\delta + \epsilon)}{12\epsilon((m^2\pi^2 - 4)\epsilon - 16\pi^2\beta)}. \tag{120}$$

(2) In-phase solution, m even:

$$v_1 = m\pi\delta + \frac{4\beta}{m}, \tag{121}$$

$$v_2 = -m\pi\delta + \frac{4\beta}{m}, \tag{122}$$

$$\phi = -\frac{\delta}{4\pi^2} + \frac{m^2\pi\delta^2}{12\epsilon} + \frac{\beta\delta}{4\pi\delta+\epsilon} + \frac{16\beta^2\delta}{m^2\epsilon(4\pi\delta+\epsilon)}, \tag{123}$$

$$\psi = \frac{m}{2} - \frac{\delta}{4\pi^2} + \frac{m^2\pi\delta^2}{12\epsilon} - \frac{\beta\delta}{4\pi\delta+\epsilon} + \frac{16\beta^2\delta}{m^2\epsilon(4\pi\delta+\epsilon)}. \tag{124}$$

(3) Out-of-phase solution, m odd:

$$v_1 = m\pi\delta + \frac{4\beta}{m} - \frac{\epsilon}{m\pi^2}, \tag{125}$$

$$v_2 = -m\pi\delta + \frac{4\beta}{m} - \frac{\epsilon}{m\pi^2}, \tag{126}$$

$$\phi = \frac{1}{2} - \frac{\beta\delta}{\epsilon} - \frac{m^4\pi^3\delta^2(4\pi\delta+\epsilon)}{12\epsilon((m^2\pi^2-4)\epsilon+16\pi^2\beta)}, \tag{127}$$

$$\psi = \frac{1}{2} + \frac{m}{2} - \frac{\beta\delta}{\epsilon} - \frac{m^4\pi^3\delta^2(4\pi\delta-\epsilon)}{12\epsilon((m^2\pi^2-4)\epsilon+16\pi^2\beta)}. \tag{128}$$

(4) Out-of-phase solution, m even:

$$v_1 = m\pi\delta + \frac{4\beta}{m}, \tag{129}$$

$$v_2 = -m\pi\delta + \frac{4\beta}{m}, \tag{130}$$

$$\phi = \frac{1}{2} - \frac{\delta}{4\pi^2} - \frac{m^2\pi\delta^2}{12\epsilon} + \frac{\beta\delta}{4\pi\delta-\epsilon} - \frac{16\beta^2\delta}{m^2\epsilon(4\pi\delta-\epsilon)}, \tag{131}$$

$$\psi = \frac{1}{2} + \frac{m}{2} - \frac{\delta}{4\pi^2} - \frac{m^2\pi\delta^2}{12\epsilon} - \frac{\beta\delta}{4\pi\delta-\epsilon} - \frac{16\beta^2\delta}{m^2\epsilon(4\pi\delta-\epsilon)}. \tag{132}$$

As before, we need to make sure our orbits have the correct itinerary. This means we must consider whether our trajectory section y_a will hit the lower boundary before $t = \psi$. This will occur if the value of v_2 we have derived is positive (recall that there can be no maxima of y in the freeplay region). Therefore we require in each case:

(1) In-phase, m odd:

$$\beta > \frac{m^2\pi\delta}{4} - \frac{\epsilon}{4\pi^2}. \tag{133}$$

(2) In-phase, m even:

$$\beta > \frac{m^2\pi\delta}{4}. \tag{134}$$

(3) Out-of-phase, m odd:

$$\beta > \frac{m^2\pi\delta}{4} + \frac{\epsilon}{4\pi^2}. \tag{135}$$

(4) Out-of-phase, m even:

$$\beta > \frac{m^2\pi\delta}{4}. \tag{136}$$

We also consider if, analogously to the $P(m,1,0)$ case, there is a boundary $\epsilon \sim \delta^2$ in parameter space, where $P(m,1,1)$ solutions cease to exist. We substitute series expansions for v_1, v_2, ϕ and ψ as above, together with modified assumptions on the parameters

$$\epsilon = \epsilon_2\delta^2, \qquad \beta = \beta_1\delta, \tag{137}$$

and again expand in the small parameter δ, solving in turn for the coefficients of the expansions. The $\mathcal{O}(\delta^2)$ terms gives rise to a consistency condition for ϕ_0,

$$\sin(2\pi\phi_0) = -\frac{\pi(\pi^2m^4 + 48\beta_1^2)}{3\epsilon_2\left(4\beta_1((-1)^m - 1) + \pi m^2((-1)^{m+1} - 1)\right)}. \tag{138}$$

Thus, for solutions to exist, the argument of the arcsin function must be less than one in modulus; which upon rearrangement leads to bounds on ϵ for the existence of $P(m,1,1)$ solutions (to leading order). Namely, $P(m,1,1)$ solutions will exist, for m odd, if

$$\epsilon > 2\pi\beta\delta + \frac{m^4\pi^3\delta^3}{24\beta}, \tag{139}$$

and, for m even, if

$$\epsilon > \frac{m^2\pi^2\delta^2}{6} + \frac{8\beta^2}{m^2}. \tag{140}$$

7.1.2 Stability

The stability of $P(m,1,1)$ solutions is given by the eigenvalues of the matrix

$$A_3 = D(\phi + m, v_1)\Phi_1(\phi - \psi + m)D(\psi, -v_2)\Phi(\psi - \phi). \tag{141}$$

As before, the algebraic expressions for eigenvalues are complicated, but they can easily be computed numerically, by substituting in parameter values that satisfy our conditions of existence for the in-phase and out-of-phase solutions. The results are illustrated in the bifurcation diagrams shown in Figures 13 and 14.

7.1.3 Bifurcations

As before we examine the eigenvalues of the Jacobian matrix (141) to locate standard bifurcations in addition to grazing bifurcations associated with the existence conditions above. The three cases we consider are:

(1) Complex conjugate Floquet multipliers on the unit circle are not possible as before.
(2) Real Floquet multiplier at -1, corresponding to period-doubling bifurcations. We again consider all possible combinations:
- In-phase, m odd:
$$\epsilon = \frac{2\pi^2(4\beta \pm m^2\pi\delta)}{m^2\pi^2 - 2}, \tag{142}$$
which has two solutions if $4\beta/(m^2\pi) > \delta$.
- In-phase, m even:
$$\epsilon = -2\pi\delta \pm \frac{8\beta}{m^2}, \tag{143}$$
of which only the '+' solution is in our region of interest.
- Out-of-phase, m odd:
$$\epsilon = \frac{2\pi^2(-4\beta \pm m^2\pi\delta)}{m^2\pi^2 - 2}, \tag{144}$$
where only the '+' solution is in our region of interest.
- Out-of-phase, m even:
$$\epsilon = 2\pi\delta \pm \frac{8\beta}{m^2}. \tag{145}$$
(3) Real Floquet multiplier at $+1$. For this the parameters must satisfy
- In-phase, m odd:
$$\epsilon = \frac{16\beta\pi^2}{m^2\pi^2 - 4}, \tag{146}$$
- In-phase, m even:
$$\epsilon = 0,\ -4\pi\delta, \tag{147}$$
therefore clearly there are no relevant lines.
- Out-of-phase, m odd:
$$\epsilon = 0,\ -\frac{16\pi^2\beta}{m^2\pi^2 - 4}, \tag{148}$$
therefore no relevant lines.
- Out-of-phase, m even:
$$\epsilon = 0,\ 4\pi\delta, \tag{149}$$
both of which are on the boundary of our region of interest.

It is clearer to see which conditions are relevant in our parameter space by examining the bifurcation diagrams in Figs. 13 and 14. Once again we see

a wide region of parameter space in which there are many stable solutions, coexisting both with the silent permanent contact solution, as well as the $P(m,1,0)$ periodic orbits. Once again, provided that $4\pi\delta - \epsilon < 16\beta$, as we increase ϵ from zero while keeping $4\pi\delta - \epsilon$ constant (following the dash/dotted lines in Figures 13 and 14) we first see a cyclic fold bifurcation at which a pair of solutions is born, one stable and one unstable, that each hits $y = \pm\beta$ once per period. The period that emerges first depends on the particular parameter values δ, ϵ and β; they are all born when $\epsilon \sim \delta^2$ however. By increasing ϵ by order of magnitude, so $\epsilon \sim \delta$, the stable $P(m,1,1)$ solutions first lose stability through a smooth period doubling, then both unstable $P(m,1,1)$ solutions are destroyed through grazing solutions, either separately (for m even) or together (for m odd). As before, these grazing bifurcations appear to meet and be organised in points $(\epsilon,\delta) = (0, 16\beta/m^2)$. These are probable codimension-two points, whose analysis we defer to further work [28].

Thus as we found before, the possible solutions to the rattle problems, predicted by our model, are to reduce the oscillatory forcing, tighten the backlash, or increase the damping. Moreover, for small damping values, large numbers of rattling solutions coexist, see Figure 15.

7.2 Piecewise linear contact model

We study again the existence and stability of $P(m,1,1)$ solutions by using a piecewise linear model of the contact force. In this case the solutions of interest can be sketched as in Fig. 16. This is the most algebraically complicated situation we shall consider.

The trajectory is now made up of four smooth parts:

$$y(t) = \begin{cases} y_a(t) & \phi < t < \phi + \sigma_1 \qquad (y > \beta), \\ y_b(t) & \phi + \sigma_1 < t < \psi \qquad (|y| < \beta), \\ y_c(t) & \psi < t < \psi + \sigma_2 \qquad (y < -\beta), \\ y_d(t) & \psi + \sigma_2 < t < \phi + m \qquad (|y| < \beta), \end{cases} \tag{150}$$

illustrated graphically in Fig. 16.

7.2.1 Existence

Solving the relevant ODEs for $y(t)$ (15)–(17) with the initial conditions indicated in Fig. 16, and applying appropriate matching conditions for continuity

of the trajectory, leads to a system

$$\boldsymbol{f}(\boldsymbol{x},\boldsymbol{p}) = \begin{bmatrix} y_a(\phi+\sigma_1)-\beta \\ y_a'(\phi+\sigma_1)+v_2 \\ y_b(\psi)+\beta \\ y_b'(\psi)+v_3 \\ y_c(\psi+\sigma)+\beta \\ y_c'(\psi+\sigma)-v_4 \\ y_d(\phi+m)-\beta \\ y_d'(\phi+m)-v_1 \end{bmatrix} = \mathbf{0}. \tag{151}$$

of eight equations in the eight unknowns $\boldsymbol{x} = [\phi, \psi, \sigma_1, \sigma_2, v_1, v_2, v_3, v_4]^T$. We solve these equations using the same asymptotic expansion techniques as before; for the sake of brevity we do not display the solutions here (see [7] for full details). As before we have sets of solutions for m odd and m even, and for in-phase and out-of-phase solutions. We again find that, to leading order, the existence criteria correspond exactly to those in the impacting case. We also find an identical condition, on existence corresponding to a fold bifurcation, as in the impacting contact model case.

7.2.2 Stability and Bifurcations

We can consider the stability of $P(m,1,1)$ solutions in the piecewise linear contact force model using the same approach followed so far; that is by studying the eigenvalues of the matrix

$$\Phi_1(\phi+m-\psi)\Phi_2(\sigma_2)\Phi_1(\psi-\phi)\Phi_2(\sigma_1), \tag{152}$$

that arises from the composition of Jacobian matrices associated to small perturbations in each of the phase-space regions. We will not attempt to find expansions for our Floquet multipliers in general. Numerical simulations show that the same stability results obtained in the impacting case are still valid. The same is true if we construct the two-parameter bifurcation diagrams using the piecewise linear model of backlash.

8 Conclusions

In this paper we have considered the dynamics of rattling motion in lightly damped geared systems. We have derived a model with particular reference

to the Roots blower vacuum pump, which we believe is also applicable to a wide range of other mechanical systems in the small damping large stiffness limit. We have derived bounds for the existence of silent solutions, and we have classified rattling periodic solutions, in which the gears repeatedly lose and re-establish contact.

We have presented a method to find analytical existence and stability boundaries for two simple classes of rattling solutions. In addition we have derived conditions for smooth bifurcations and non-smooth transitions of periodic orbits, and hence produced bifurcation diagrams. All this analysis has been performed for both the impacting and piecewise linear backlash models. We have shown that to leading order in the small damping parameter, both backlash models produce the same existence, stability and two-parameter bifurcation diagrams. We have yet to fully unfold the points which act as organising centres for many of the bifurcations; for a preliminary study see [28].

We can validate our findings by integrating the equation of motion (14) numerically. Our analysis predicts that there are coexisting stable periodic orbits of type $P(m, 1, 0)$ and $P(m, 1, 1)$ for suitable choices of parameters; we can also use our construction techniques to generate suitable initial conditions. We show in Fig. 17 time integration plots of the PWL contact model, for representative parameter values $\delta = 0.5 \times 10^{-4}$, $\epsilon = 10^{-4}$, $\beta = 6 \times 10^{-4}$ and $\kappa = 10^{8}$, differing only in the choice of initial conditions. We do indeed see coexisting stable solutions of both types, all of which also coexist with the permanent contact solution, confirming our theoretical predictions.

We have thus shown the importance of full nonlinear analysis in machine design. In particular, a machine may be capable of silent (linear) motion but have coexisting rattling modes of operation which are noisy. Moreover, we have analysed only a few of the possible families of periodic solutions, and there may exist more complicated types of solution such as quasi-periodic or chaotic. In the analysis presented here, these modes can only be destroyed by either increasing the damping or substantially reducing the amplitude of the oscillatory forcing, and these approaches may be neither possible (from the point of view of manufacturing tolerances) nor satisfactory (e.g. from the point of view of power consumption). However, in practice, limitations in our modelling, such as the neglexion of lubrication, will modify the story presented here.

A further technical issue concerns the basins of attraction of some of the stable rattling solutions that we have presented. We believe that some of these are vanishingly small in the small damping limit, and hence will not have an influence on real machine dynamics. This is an issue which we defer to further work.

Acknowledgements

The authors gratefully acknowledge the financial support of the Engineering and Physical Sciences Research Council, Jaguar Cars and BOC Edwards. We would also like to thank Alan Champneys and Jo Mason for useful discussions.

References

[1] S. Theodossiades, S. Natsiavas, Non-linear dynamics of gear-pair systems with periodic stiffness and backlash, J. Sound Vib. 229 (2) (2000) 287–310.

[2] G. Litak, M. I. Friswell, Vibration in gear systems, Chaos, Solitons, Fractals 16 (5).

[3] N. Sarkar, R. E. Ellis, T. N. Moore, Backlash detection in geared mechanisms: Modeling, simulation, and experimentation, Mech. Sys. Signal Proc. 11 (3) (1997) 391–408.

[4] J. Mason, Mathematical modelling of gear rattle in dual-shaft vacuum pumps, Master's thesis, University of Bristol (2005).

[5] H. Berges, D. Gotz, Oil-free vacuum pumps of compact design, Vacuum 38 (1988) 761–763.

[6] M. H. Hablanian, Design and performance of oil-free pumps, Vacuum 41 (1990) 1814–1818.

[7] C. K. Halse, Nonlinear dynamics of the automotive driveline, Ph.D. thesis, University of Bristol (2004).

[8] P. Couderc, J. Callenaere, J. D. Hagopian, G. Ferraris, A. Kassai, Y. Borjesson, L. Verdillon, S. Gaimard, Vehicle driveline dynamic behaviour: Experimentation and simulation, J. Sound Vib. 218 (1) (1998) 133–157.

[9] Z. H. Wang, D. J. Wang, Dynamic characteristics of a rolling mill drive system with backlash in rolling slippage, J. Mat. Proc. Tech. 97 (1-3) (2000) 69–73.

[10] D. H. Gonsalves, R. D. Neilson, A. D. S. Barr, A study of the response of a discontinuously nonlinear rotor system, Nonlin. Dyn. 7 (4) (1995) 451–470.

[11] I. Roberts, D. P. Jones, N. A. J. Lieven, M. di Bernado, A. R. Champneys, Analysis of piecewise linear aeroelastic systems using numerical continuation, Proc. Inst. Mech. Eng. G 216 (G1) (2002) 1–11.

[12] Z. T. Zhusubaliyev, E. A. Soukhoterin, Oscillations in a relay control system with hysteresis and time dead zone, Math. Comp. Sim. 58 (4-6) (2002) 329–350.

[13] I. A. Mahfouz, F. Badrakhan, Chaotic behaviour of some piecewise-linear systems. Part 2: systems with clearance, J. Sound Vib. 143 (2) (1990) 289–328.

[14] M. Kleczka, E. Kreuzer, W. Schiehlen, Local and global stability of a piecewise linear oscillator, Phil. Trans. Roy. Soc. 338 (1651) (1992) 533–546.

[15] M. Wiercigroch, Bifurcation analysis of a harmonically excited linear oscillator with clearance, Chaos, Solitons, Fractals 4 (2) (1994) 297–303.

[16] M. Wiercigroch, V. W. T. Sin, Measurement of chaotic vibration in symmetrical piecewise linear oscillator, Chaos, Solitons, Fractals 9 (1/2) (1998) 209–220.

[17] A. C. J. Luo, S. Menon, Global chaos in a periodically forced, linear system with a dead-zone restoring force, Chaos, Solitons, Fractals 19 (5) (2004) 1189–1199.

[18] Y. A. Kuznetsov, Elements of Applied Bifurcation Theory, 2nd Edition, Springer-Verlag, New York, 1998.

[19] M. di Bernardo, C. Budd, A. Champneys, P. Kowalczyk, A. Nordmark, G. Olivar, P. Piiroinen, Bifurcations in nonsmooth dynamical systems, SIAM Review.

[20] P. Kowalczyk, M. di Bernardo, A. R. Champneys, S. J. Hogan, M. Homer, Y. A. Kuznetsov, A. Nordmark, P. T. Piiroinen, Two-parameter nonsmooth bifurcations of limit cycles: classification and open problems, Int. J. Bif. Chaos.

[21] B. Brogliato, Nonsmooth Mechanics, Springer-Verlag, 1999.

[22] A. H. Nayfeh, B. Balachandran, Applied Nonlinear Dynamics, John Wiley & Sons Inc., 1994.

[23] A. Nordmark, Non-periodic motion caused by grazing incidence in impact oscillators, J. Sound Vib. 145 (2) (1991) 279–297.

[24] A. Nordmark, Universal limit mapping in grazing bifurcations, Phys. Rev. E 55 (1997) 62–82.

[25] H. Dankowicz, A. Nordmark, On the origin of stick-slip bifurcations, Physica D 136 (2000) 280–312.

[26] P. Piiroinen, Recurrent dynamics of nonsmooth systems with application to human gait, Ph.D. thesis, Royal Institute of Technology, Stockholm (2002).

[27] M. B. Monagan, K. O. Geddes, K. M. Heal, G. Labahn, S. Vorkoetter, Maple V programming guide, Springer-Verlag, 1996.

[28] C. Halse, R. E. Wilson, M. di Bernardo, M. Homer, Numerical bifurcation analysis of a single degree of freedom gear model, in progress.

[29] H. E. Merritt, Gear Engineering, Pitman Publishing, 1971.

List of Figures

1 Schematic diagram of the moving parts of a Roots blower vacuum pump, illustrating the parallel arrangement of rotors, shafts and gears. 39

2 The three modes of gear meshing (full details are given in [29]). From left to right: (a) X drives Y, (b) Freeplay, (c) Y drives X. In state (a) the gears are in contact, with the X-shaft driving the Y-shaft. (b) illustrates 'freeplay'; in this state there is no contact between the gears. (c) shows torque reversal, where the Y-shaft drives the X-shaft. 40

3 The external torques acting on the shafts of meshing gears. The right hand side drawing illustrates the interaction force between the gears. 41

4 Sketch of a permanent contact solution with backlash width $\beta = 0.1$. 42

5 Backlash models. 43

6 Transformation of parameter space. 44

7 Sketches of some different types of solutions: (a) $P(1,1,0)$ out-of-phase, (b) $P(1,1,1)$ in-phase, (c) $P(2,1,1)$ out-of-phase. 45

8 Notation for the $P(m,1,0)$ solution with the impacting contact model. 46

9 Sketch of bifurcations of $P(m,1,0)$ solutions for the impacting contact model, m odd. As we vary parameters along the vertical dash-dot line we observe a sequence of bifurcations: first a cyclic-fold where the unstable and stable solutions are created, then a grazing where the stable solution impacts the boundary at $y = -\beta$, and finally a grazing where the unstable solution impacts the boundary at $y = -\beta$. 47

10 Sketch of bifurcations of $P(m,1,0)$ solutions for the impacting contact model, m even. As we vary parameters along the vertical dash-dot line we observe a sequence of bifurcations: first a cyclic-fold where the unstable and stable solutions are born, and then a simultaneous (to $\mathcal{O}(\delta^2)$) grazing of both solutions with the boundary $y = -\beta$. 47

11 Notation for the $P(m,1,0)$ solution with the PWL contact model. 48

12 Sketch of a $P(1,1,1)$ orbit, impacting contact model. 49

13 Sketch of bifurcations of $P(m,1,1)$ solutions, odd period. As we follow the dash-dotted line we have a cyclic-fold bifurcation where the unstable and stable solutions are born, then a period-doubling bifurcation where the stable solution becomes unstable. This unstable solution then grazes the boundary at $y=-\beta$ before the original unstable solution grazes the boundary $y=-\beta$. 50

14 Sketch of bifurcations of $P(m,1,1)$ solutions, even period. As we follow the dash-dotted line we have a cyclic-fold bifurcation where the unstable and stable solutions are born, then a period-doubling bifurcation where the stable solution becomes unstable, and finally both unstable solutions simultaneously (to $\mathcal{O}(\delta^2)$) graze the boundary $y=-\beta$. 50

15 Scale diagram of the regions of existence of stable solutions for $m=1,2,3,4$, $\beta=6\times10^{-4}$. The number of solutions increases as we approach the origin. The locations of the cyclic-fold bifurcations are not shown as they are too close to the $(4\pi\delta-\epsilon)$-axis to be visible. 51

16 Sketch of a $P(1,1,1)$ orbit, piecewise linear contact model. 52

17 Numerical integration of (14) showing coexisting stable $P(m,1,0)$ and $P(m,1,1)$ solutions for $m=1,2,3$ with the piecewise linear contact model, $\delta=0.5\times10^{-4}$, $\epsilon=10^{-4}$, $\beta=6\times10^{-4}$, $\kappa=10^{8}$. These solutions all coexist with the permanent contact solution, a sinusoid of amplitude $\epsilon/(2\kappa)$ centred at $y=\beta+2\pi\delta/\kappa$. 53

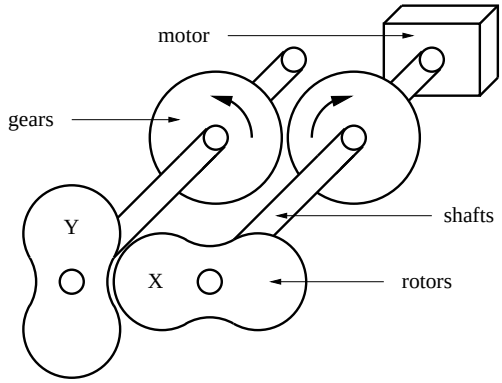

Fig. 1. Schematic diagram of the moving parts of a Roots blower vacuum pump, illustrating the parallel arrangement of rotors, shafts and gears.

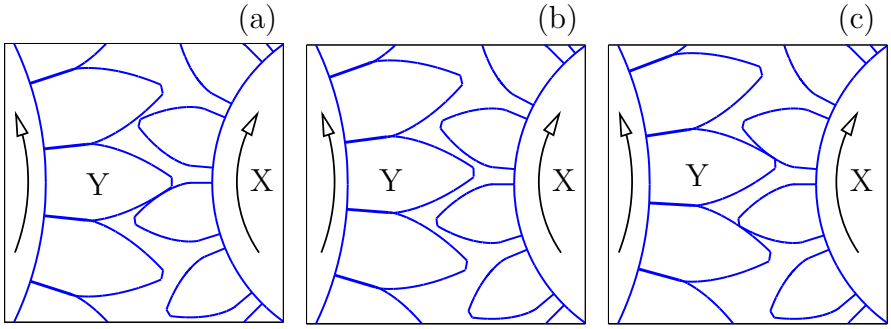

Fig. 2. The three modes of gear meshing (full details are given in [29]). From left to right: (a) X drives Y, (b) Freeplay, (c) Y drives X. In state (a) the gears are in contact, with the X-shaft driving the Y-shaft. (b) illustrates 'freeplay'; in this state there is no contact between the gears. (c) shows torque reversal, where the Y-shaft drives the X-shaft.

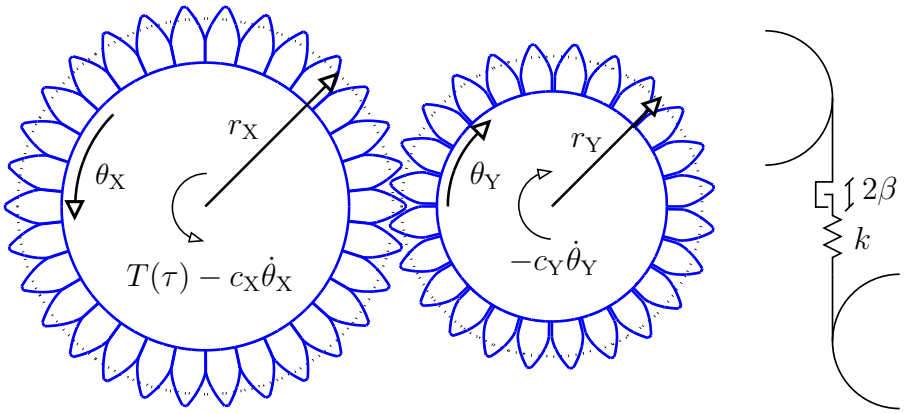

Fig. 3. The external torques acting on the shafts of meshing gears. The right hand side drawing illustrates the interaction force between the gears.

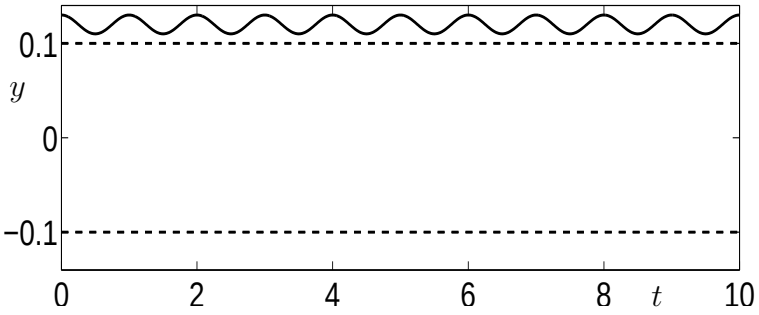

Fig. 4. Sketch of a permanent contact solution with backlash width $\beta = 0.1$.

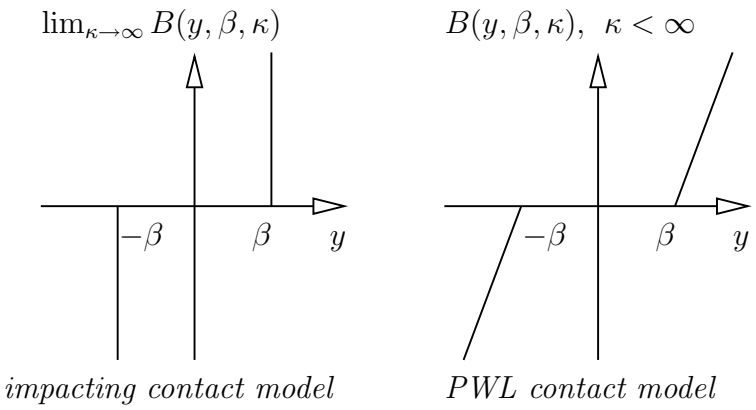

Fig. 5. Backlash models.

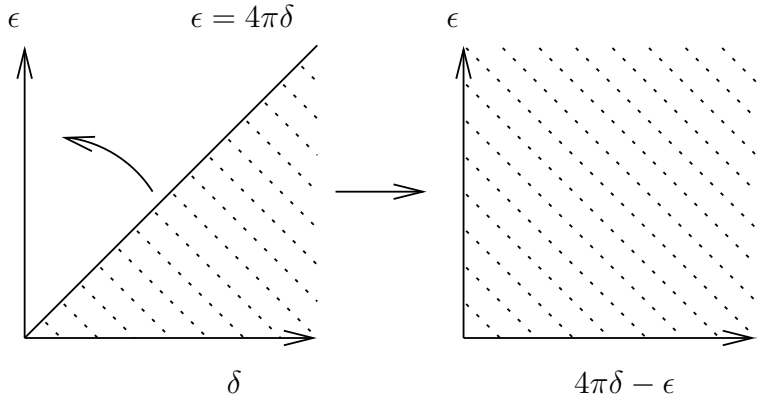

Fig. 6. Transformation of parameter space.

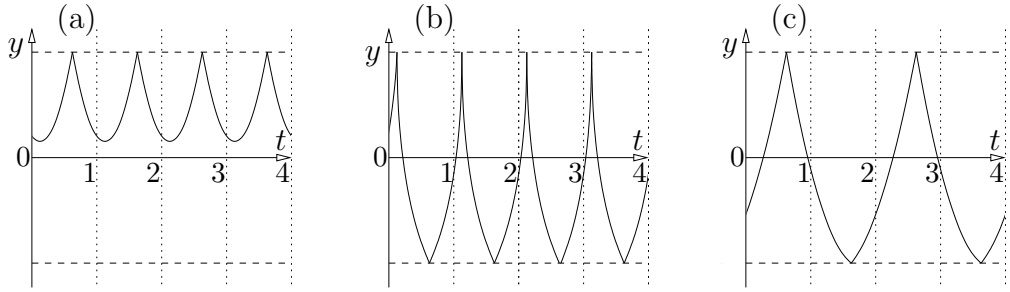

Fig. 7. Sketches of some different types of solutions: (a) $P(1,1,0)$ out-of-phase, (b) $P(1,1,1)$ in-phase, (c) $P(2,1,1)$ out-of-phase.

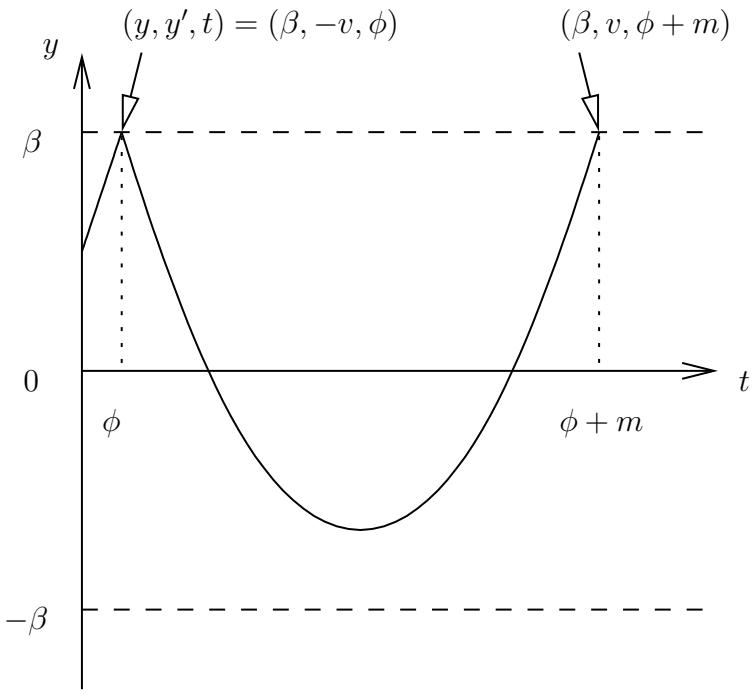

Fig. 8. Notation for the $P(m, 1, 0)$ solution with the impacting contact model.

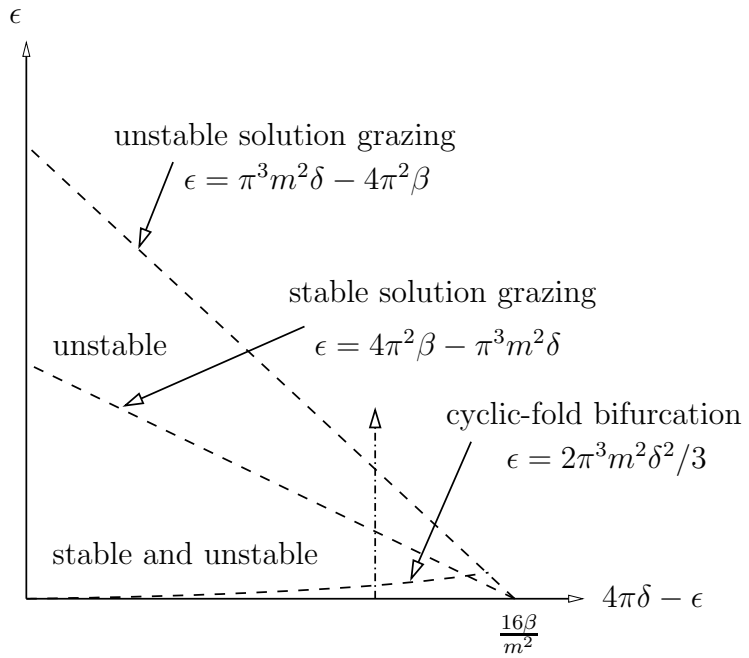

Fig. 9. Sketch of bifurcations of $P(m, 1, 0)$ solutions for the impacting contact model, m odd. As we vary parameters along the vertical dash-dot line we observe a sequence of bifurcations: first a cyclic-fold where the unstable and stable solutions are created, then a grazing where the stable solution impacts the boundary at $y = -\beta$, and finally a grazing where the unstable solution impacts the boundary at $y = -\beta$.

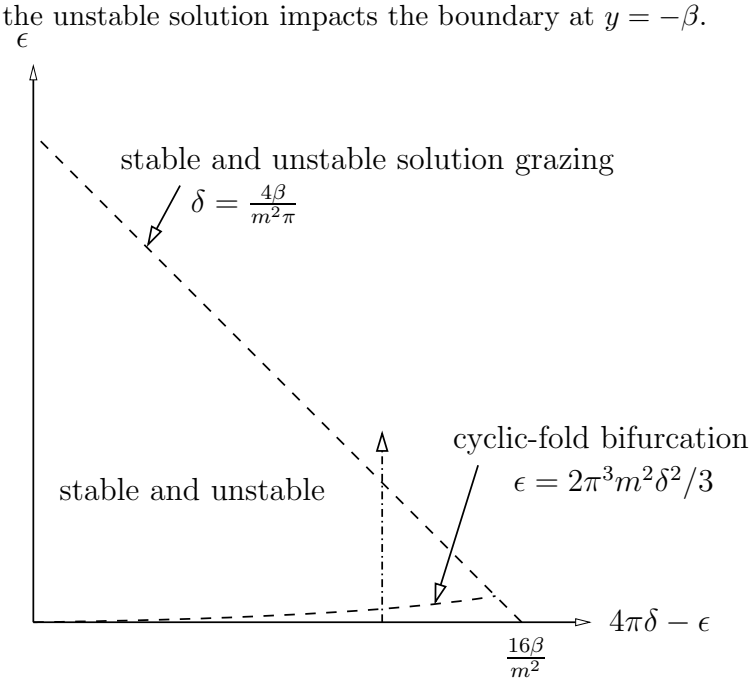

Fig. 10. Sketch of bifurcations of $P(m, 1, 0)$ solutions for the impacting contact model, m even. As we vary parameters along the vertical dash-dot line we observe a sequence of bifurcations: first a cyclic-fold where the unstable and stable solutions are born, and then a simultaneous (to $\mathcal{O}(\delta^2)$) grazing of both solutions with the boundary $y = -\beta$.

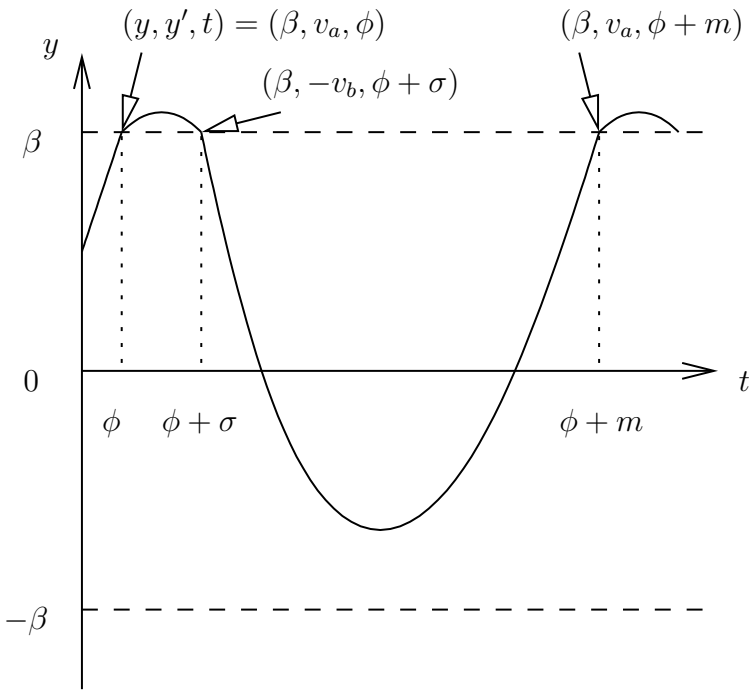

Fig. 11. Notation for the $P(m, 1, 0)$ solution with the PWL contact model.

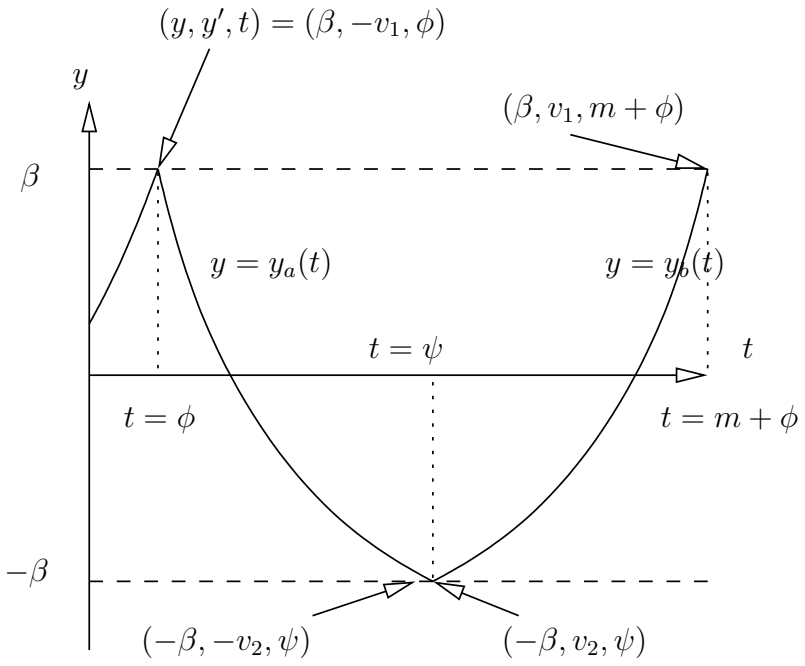

Fig. 12. Sketch of a $P(1, 1, 1)$ orbit, impacting contact model.

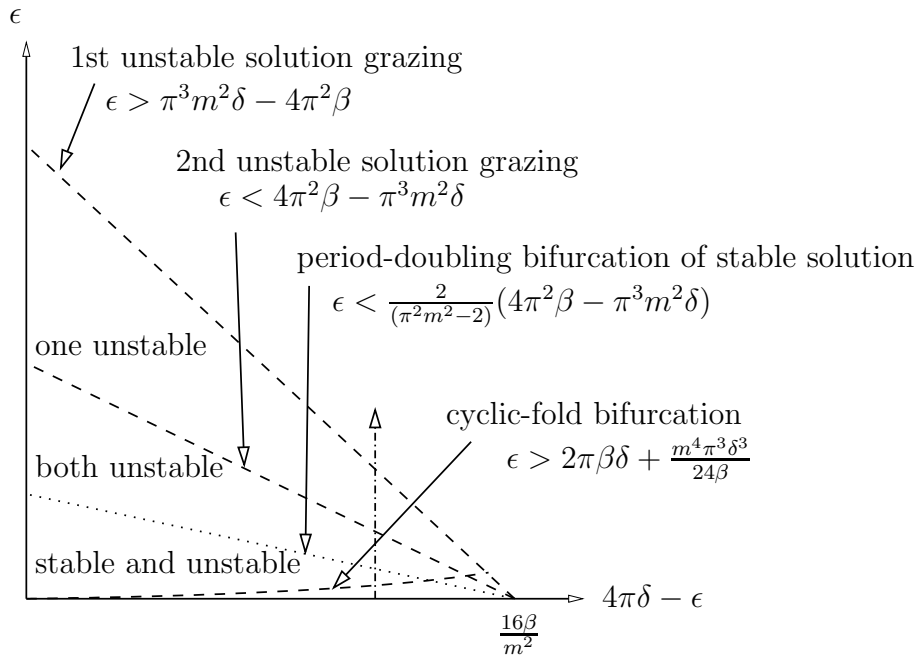

Fig. 13. Sketch of bifurcations of $P(m, 1, 1)$ solutions, odd period. As we follow the dash-dotted line we have a cyclic-fold bifurcation where the unstable and stable solutions are born, then a period-doubling bifurcation where the stable solution becomes unstable. This unstable solution then grazes the boundary at $y = -\beta$ before the original unstable solution grazes the boundary $y = -\beta$.

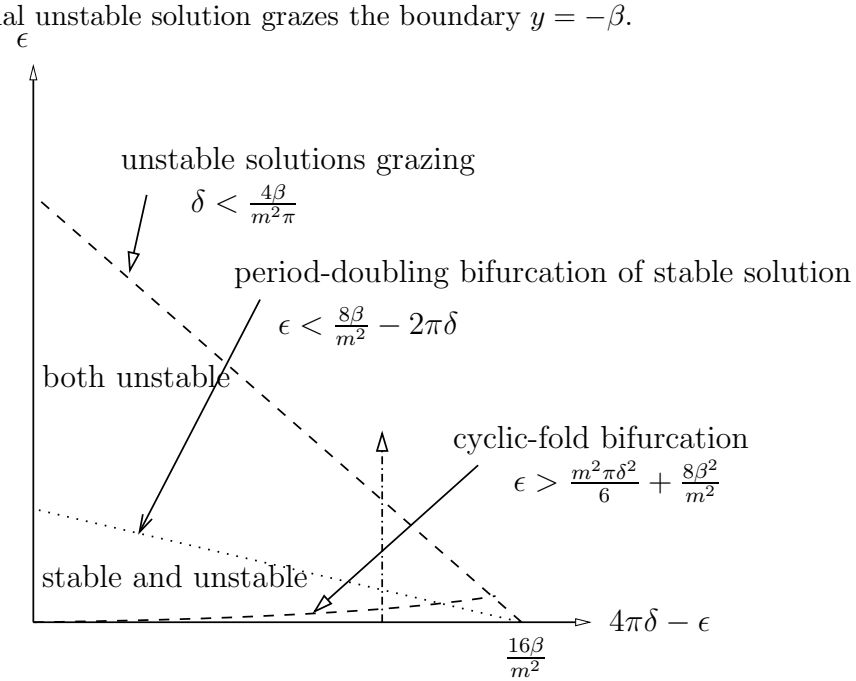

Fig. 14. Sketch of bifurcations of $P(m, 1, 1)$ solutions, even period. As we follow the dash-dotted line we have a cyclic-fold bifurcation where the unstable and stable solutions are born, then a period-doubling bifurcation where the stable solution becomes unstable, and finally both unstable solutions simultaneously (to $\mathcal{O}(\delta^2)$) graze the boundary $y = -\beta$.

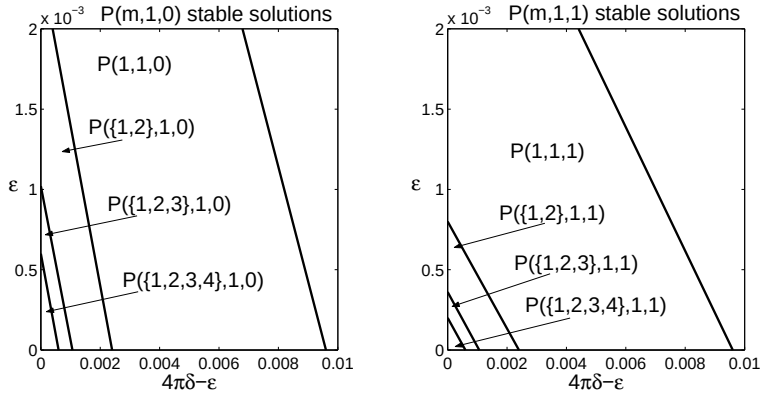

Fig. 15. Scale diagram of the regions of existence of stable solutions for $m = 1, 2, 3, 4$, $\beta = 6 \times 10^{-4}$. The number of solutions increases as we approach the origin. The locations of the cyclic-fold bifurcations are not shown as they are too close to the $(4\pi\delta - \epsilon)$-axis to be visible.

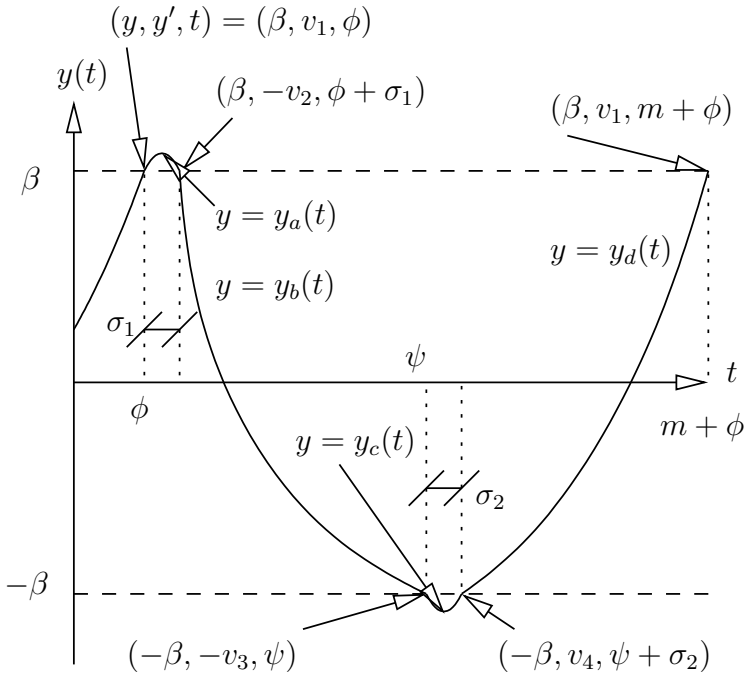

Fig. 16. Sketch of a $P(1, 1, 1)$ orbit, piecewise linear contact model.

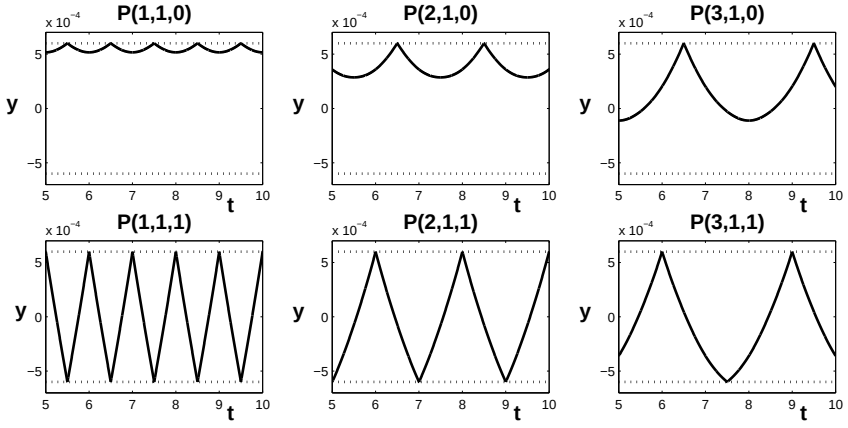

Fig. 17. Numerical integration of (14) showing coexisting stable $P(m,1,0)$ and $P(m,1,1)$ solutions for $m = 1,2,3$ with the piecewise linear contact model, $\delta = 0.5 \times 10^{-4}$, $\epsilon = 10^{-4}$, $\beta = 6 \times 10^{-4}$, $\kappa = 10^{8}$. These solutions all coexist with the permanent contact solution, a sinusoid of amplitude $\epsilon/(2\kappa)$ centred at $y = \beta + 2\pi\delta/\kappa$.